Journal of Instrumentation

PAPER • **OPEN ACCESS**

Performance of CMS muon reconstruction from proton-proton to heavy ion collisions

To cite this article: A. Hayrapetyan *et al* 2024 *JINST* **19** P09012

View the article online for updates and enhancements.

Published by IOP Publishing for Sissa Medialab

Received: *April 26, 2024*
Revised: *July 4, 2024*
Accepted: *August 12, 2024*
Published: *September 6, 2024*

Performance of CMS muon reconstruction from proton-proton to heavy ion collisions

The CMS collaboration

E-mail: cms-publication-committee-chair@cern.ch

Abstract: The performance of muon tracking, identification, triggering, momentum resolution, and momentum scale has been studied with the CMS detector at the LHC using data collected at $\sqrt{s_{\mathrm{NN}}} = 5.02$ TeV in proton-proton (pp) and lead-lead (PbPb) collisions in 2017 and 2018, respectively, and at $\sqrt{s_{\mathrm{NN}}} = 8.16$ TeV in proton-lead (pPb) collisions in 2016. Muon efficiencies, momentum resolutions, and momentum scales are compared by focusing on how the muon reconstruction performance varies from relatively small occupancy pp collisions to the larger occupancies of pPb collisions and, finally, to the highest track multiplicity PbPb collisions. We find the efficiencies of muon tracking, identification, and triggering to be above 90% throughout most of the track multiplicity range. The momentum resolution and scale are unaffected by the detector occupancy. The excellent muon reconstruction of the CMS detector enables precision studies across all available collision systems.

Keywords: Instrumentation and methods for heavy-ion reactions and fission studies; Large detector systems for particle and astroparticle physics; Muon spectrometers

ArXiv ePrint: 2404.17377

https://doi.org/10.1088/1748-0221/19/09/P09012

2024 JINST 19 P09012

Contents

1 Introduction

An estimate of the capability of a detector to reconstruct and identify particles of interest is essential to ensure the reliability of the data and the precision of measurements. A crucial measure of the performance of both the detector and its reconstruction algorithms is the efficiency, which is a required correction for any measurement of cross sections or particle yields. Efficiency is defined as a fraction of a given species of particles within the detector acceptance that are successfully reconstructed with a given set of selection criteria. The efficiency could be estimated using Monte Carlo (MC) simulations, where the particles present in the event are known a priori. However, estimates from MC simulations assume an accurate description of a detector and its interaction processes, which may have characteristics that are challenging to quantify. Rather than relying solely on detector simulations, data-driven approaches for estimating efficiencies have been developed. We use the

2024 JINST 19 P09012

data-driven tag-and-probe method that has been successfully used in various analyses in proton-proton (pp), proton-lead (pPb), and lead-lead (PbPb) collisions performed by the CMS detector at the CERN Large Hadron Collider (LHC) [1–3]. Performance studies of the CMS detector have been carried out since the beginning of LHC operations in pp collisions [4, 5], and we now extend these studies to pPb and PbPb collisions.

We use heavy ion collisions to gain insight into the collective thermodynamic properties of cold and hot QCD matter, including the color-deconfined quark-gluon plasma (QGP) [6]. Resonances that decay into muons (e.g., J/ψ, Υ, Z) provide information about the QGP, because its presence has measurable effects on particle yields and distributions. Muon measurements are more challenging in the high-occupancy environments of heavy ion collisions. One quantifiable indicator of occupancy is the charged particle multiplicity of the event, which in PbPb collisions is highly correlated with the collision impact parameter (distance between the centers of the two nuclei in the plane perpendicular to the beam line). For the collisions with near-zero impact parameter (central events), the multiplicities can be hundreds of times larger than those observed in a single pp collision [7]. These central events result in extremely high multiplicity per unit area, especially in the innermost CMS subdetectors used for tracking. Consequently, any degradation in tracking performance is likely to affect the muon measurements, despite the fact that the occupancies in the outermost CMS muon subdetectors remain low.

In this paper we report on the performance of muon reconstruction, identification (ID), triggering, dimuon-mass resolution, and dimuon-mass scale. The reference physical processes are the decays of Z and J/ψ resonances, whose decay muons cover a wide kinematic range, thus providing a good data sample for measuring the muon performance in the CMS detector. The efficiencies are estimated using a tag-and-probe method, which is described in detail in section 5. The efficiencies are reported in sections 6–8; the mass resolution and scale are presented in section 9. We summarize the paper in section 10.

2 CMS detector

A detailed description of the CMS detector is reported in ref. [8]. A schematic view of the detector is shown in figure 1. Muon reconstruction is performed using the all-silicon inner tracker at the center of the detector immersed in a 3.8 T solenoidal magnetic field, and with up to four stations of gas-ionization muon detectors installed outside the solenoid and sandwiched between the layers of the steel flux-return yoke. The inner tracker is composed of a pixel detector and a silicon strip tracker, and measures charged-particle trajectories in the pseudorapidity range $|\eta| < 2.5$. The muon system covers the pseudorapidity region $|\eta| < 2.4$ and performs three main tasks: triggering on muons, identifying muons, and improving the momentum measurement and charge determination of high transverse momentum (p_{T}) muons. Drift tube (DT) detectors and cathode strip chambers (CSC) detect muons in the η regions of $|\eta| < 1.2$ and $0.9 < |\eta| < 2.4$, respectively, and are complemented by a system of resistive-plate chambers (RPC) covering the range of $|\eta| < 1.9$. The coverage of the DT and CSC detectors defines three regions, referred to as barrel ($|\eta| < 0.9$), overlap ($0.9 < |\eta| < 1.2$), and endcap ($1.2 < |\eta| < 2.4$) regions. The electromagnetic calorimeter (ECAL) and the hadron calorimeter (HCAL), divided into barrel and endcap sections, are also shown in figure 1. The hadron forward (HF) calorimeters extend the absolute pseudorapidity range of the HCAL to 5.0, and are commonly used in trigger algorithms and estimates of the collision impact parameter.

2024 JINST 19 P09012

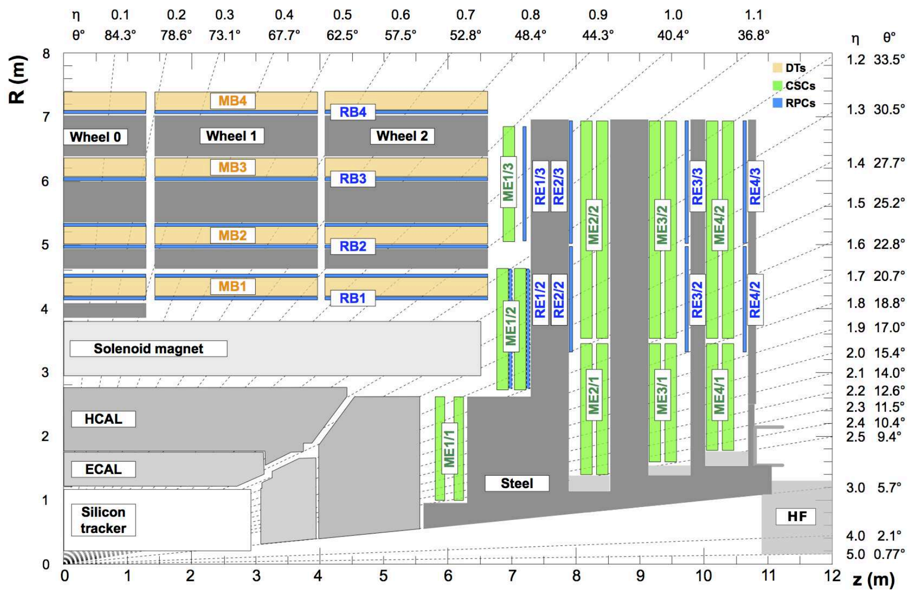

Figure 1. Longitudinal layout of one quadrant of the CMS detector. The drawing shows four DT stations in the muon barrel (MB1–MB4, yellow), four CSC stations in the muon endcap (ME1–ME4, green) and the RPC stations (RB1–RB4 and RE1–RE4, blue).

Events of interest are acquired using a two-tiered trigger system [9]. The first level (L1), composed of custom hardware processors, uses information from the calorimeters and muon detectors to select events at a rate of around 100 kHz for pp and pPb collisions (30 kHz for PbPb collisions) within a fixed latency of 4 μs [10]. The second level, known as the high-level trigger (HLT), consists of a farm of processors running a version of the full event reconstruction software optimized for fast processing. The HLT algorithms, which are seeded by the L1 triggers, further reduce the rate of data collection to around 24 kHz for the pp collisions used in this study. The corresponding HLT rate is up to 20 kHz for pPb collisions and 7 kHz for PbPb collisions.

3 Data and Monte Carlo samples

The data used in this paper were taken during the dedicated heavy ion run periods of Run 2 between 2016 and 2018. The events were recorded from pPb collisions in 2016 at a nucleon-nucleon center-of-mass energy of $\sqrt{s_{\mathrm{NN}}} = 8.16$ TeV, from pp collisions in 2017 at $\sqrt{s} = 5.02$ TeV, and from PbPb collisions in 2018 at $\sqrt{s_{\mathrm{NN}}} = 5.02$ TeV. In addition, a smaller pPb data sample at $\sqrt{s_{\mathrm{NN}}} = 5.02$ TeV was collected in 2016, which allowed us to quantify the difference between 5.02 TeV and 8.16 TeV collisions. All studied events are from hadronic collisions.

Results from the data are compared with those obtained from MC samples, in which the simulation includes the full CMS detector response using the GEANT4 package [11]. The software used to generate the nucleon-nucleon interactions that produce the particle of interest depends on the process and collision system: for J/ψ mesons we use PYTHIA8 (v2.3.0) [12]; for Z bosons in PbPb, pPb, and pp collisions we use MADGRAPH5_aMC@NLO (v2.4.2) [13], POWHEG v2 [14–17], and PYTHIA8, respectively. Differences in the details of the simulation of the hard process have a negligible impact on the studies presented in this paper. In the case of the pPb and PbPb MC samples, the

2024 JINST 19 P09012

hard-scattering nucleon-nucleon events were embedded into an underlying heavy ion collision that was simulated with either EPOS LHC (v3400) [18] (pPb) or HYDJET v1.9 [19] (PbPb). After the detailed simulation of the CMS detector response with GEANT4, MC events were processed through the trigger emulation and reconstructed by the same algorithms that were used for the collision data sample for a given year and collision system.

3.1 Possible effects of detector and alignment changes

The reconstruction performance is influenced not only by varying the collision system from pp to PbPb, but also by the changes in the detector during the years when the data were collected. The most significant addition affecting the data was the pixel-detector upgrade after the pPb data-taking period at the end of 2016. As part of the upgrade, an extra layer was added to the pixel detector in the midrapidity region, and an additional disk was added to both sides of the tracker [20].

The alignment conditions in the pixel and silicon-strip tracker detector differ across the data sets as well. The pPb and PbPb samples considered here were reconstructed using the alignment configurations that were derived during data taking. In contrast, the pp sample takes advantage of the improved end-of-year reconstruction, in which the alignment constants are rederived using the data collected during the entire year. Two examples of measurements that could be sensitive to the alignment conditions are those of the mass scale and of the mass resolution (section 9). The details of the alignment procedure and the effects of the alignment conditions on the Z boson mass reconstructed via muons were studied in ref. [21]. Although the Z boson decays are used in the alignment procedure, its mass is not fixed to a specific value. In particular, the alignment parameters obtained for a given system are identical irrespective of the multiplicity of the collision. Hence, the Z boson remains a useful probe into differences in resolution and scale. It was verified in one of the studies discussed in ref. [21] that the difference in the reconstructed Z boson mass between the alignment conditions derived during data taking and those derived at the end of the year was $\lesssim 0.1\%$. Based on the small size of the effect, we conclude that the alignment differences do not significantly affect the comparisons among the pp, pPb, and PbPb data sets.

4 Muons in the heavy ion environment

The main difference among the collision systems that affects the detector performance is the number of charged particles produced per collision. The variable N_{tracks}, which is obtained by counting tracks in the pseudorapidity range $|\eta| < 2.4$, characterizes the total charged particle multiplicity. The distributions of N_{tracks} in pp, pPb, and PbPb collision events are shown in the left panel of figure 2. In PbPb collisions, events with a large number of tracks correspond to the most central collisions (large nucleus-nucleus overlap, small impact parameter), whereas a small number of tracks indicates a peripheral collision (small nucleus-nucleus overlap, large impact parameter). Centrality is a variable used to characterize the amount of overlap between colliding nuclei. The centrality bins are given in percentile ranges of the total inelastic hadronic cross section, calculated from the energy deposited in the HF calorimeters, such that 0% centrality corresponds to the most central collisions and 100% corresponds to the most peripheral (see ref. [22], figure 3, where the centrality definition used in CMS is discussed). To illustrate the highest multiplicities achievable in PbPb collisions, the distribution of N_{tracks} in the 0–20% most central PbPb collisions is shown in green. Similarly, larger multiplicities than those of pp collisions are seen in the pPb system. We also compare the N_{tracks} distributions

2024 JINST 19 P09012

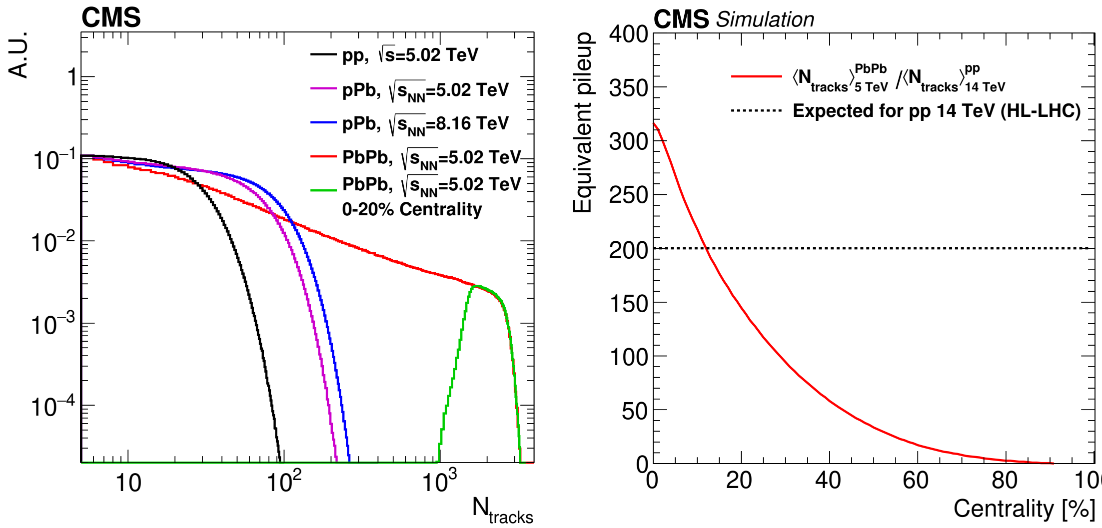

Figure 2. Left: Distribution of N_{tracks} in pp collisions at $\sqrt{s}$ = 5.02 TeV (black); pPb collisions at $\sqrt{s_{\text{NN}}}$ = 5.02 TeV (magenta) and at 8.16 TeV (blue); and PbPb collisions at $\sqrt{s_{\text{NN}}}$ = 5.02 TeV (red). The distribution of N_{tracks} in the 0–20% most central PbPb collisions is shown in green. The values are not corrected for efficiency. Right: Translation of the centrality in PbPb collisions at $\sqrt{s_{\text{NN}}}$ = 5.02 TeV into an equivalent pileup in pp collisions at $\sqrt{s}$ = 14 TeV.

for pPb collisions at $\sqrt{s_{\text{NN}}}$ = 5.02 TeV and at 8.16 TeV. We see that an increase of 63% in $\sqrt{s_{\text{NN}}}$ results, on average, in the creation of 24% more tracks.

The pp collisions involve only two participating nucleons. However, pileup (mean number of collisions per bunch crossing) is significant in the pp environment due to the high instantaneous luminosities, and this affects the shape and extent of the N_{tracks} distribution. Even with pileup, the pp collisions analyzed in this paper generate far fewer tracks than PbPb and pPb collisions. The average number of reconstructed tracks in a given event, $\langle N_{\text{tracks}}\rangle$, in PbPb collisions at $\sqrt{s_{\text{NN}}}$ = 5.02 TeV corresponding to each centrality range is tabulated in table 1, and the procedure for obtaining the $\langle N_{\text{tracks}}\rangle$ is described in appendix A. The pileup for each collision system is shown in table 2, which also shows other important characteristics of the collisions discussed in this paper. The pileup in PbPb collisions is negligible, but must be taken into account in pp collisions. The multiplicities quoted in table 1 include pileup present in the event. As seen in the table, the 0–10% most central PbPb collisions have an average number of tracks $\langle N_{\text{tracks}}\rangle_{0\text{–}10\%}$ = 2345. Taking the pileup into account (3 collisions per bunch crossing, as noted in table 2), a single pp collision at $\sqrt{s}$ = 5.02 TeV has an average multiplicity of $\langle N_{\text{tracks}}\rangle \approx 19/3 \approx 6$. This makes the multiplicity in each 0–10% central PbPb event roughly equivalent to $2345/6 \approx 400$ pp collisions occurring simultaneously. The equivalent pileup, $\langle N_{\text{tracks}}\rangle_{\text{PbPb}}/\langle N_{\text{tracks}}\rangle_{\text{pp}}$, for a given PbPb collision centrality is plotted in the right panel of figure 2 as a red curve. The calculation uses a simulation of pp collisions at the highest planned energy for the LHC, 14 TeV, instead of 5.02 TeV. The increase in multiplicity due to this greater pp energy results in a smaller equivalent pileup for the most central PbPb events of ≈300. The expected pileup for pp collisions in the high-luminosity phase is 200, shown as a black dashed line. Therefore, the central PbPb collisions correspond to charged particle multiplicities that exceed those expected even in the high-luminosity phase of the LHC.

Table 1. Average number of reconstructed tracks, $\langle N_{\text{tracks}} \rangle$, in our data sets. The values are not corrected for pileup nor efficiency. Two columns are shown for PbPb collisions. The left column shows the values that are obtained from a minimum-bias data set, and correspond to distributions shown in the left panel of figure 2. The right column shows the values in muon-triggered data, and correspond to the location of points shown in the performance plots of this paper. The values for pPb are for illustrative purposes only; pPb results are binned directly in N_{tracks}. Details of the centrality conversion to $\langle N_{\text{tracks}} \rangle$ are provided in appendix A.

		$\langle N_{\text{tracks}} \rangle$	
System	Centrality range	minimum-bias	muon-triggered
PbPb, $\sqrt{s_{\text{NN}}} = 5.02$ TeV	0–10%	2345	2397
	10–20%	1721	1782
	20–30%	1224	1271
	30–40%	819	865
	40–50%	503	536
	50–60%	279	299
	60–100%	33	112
pPb, $\sqrt{s_{\text{NN}}} = 5.02$ TeV		39	
pPb, $\sqrt{s_{\text{NN}}} = 8.16$ TeV		48	
pp, $\sqrt{s} = 5.02$ TeV		19	

Table 2. Characteristics of selected collisions collected during LHC Run 2. More information on the corresponding luminosity measurements can be found in refs. [23–26].

System	pPb	pp	PbPb
Year	2016	2017	2018
$\sqrt{s_{\text{NN}}}$ (TeV)	8.16	5.02	5.02
Bunch spacing (ns)	100–200	25	75–150
Average pileup	0.25	3	0.0004
Peak instantaneous luminosity ($\text{cm}^{-2}\text{s}^{-1}$)	8×10^{29}	1×10^{34}	6×10^{27}
Integrated luminosity (nb^{-1})	1.73×10^{2}	3.04×10^{5}	1.70
Peak interaction rate (kHz)	2×10^{3}	4×10^{4}	50

A typical dimuon event in the heavy ion environment is displayed in figure 3. The inner part of the detector reconstructs the large number of tracks produced in the collision, shown as blue lines in the figure. The electromagnetic and hadronic energy captured by the calorimeters is shown as the semitransparent towers surrounding the inner tracks (the endcap calorimeters are hidden for clarity). Most of the event activity is contained within the inner detectors. Two muons are displayed as two long red tracks reaching the outermost part of the detector, where the muon chambers are located. The high occupancy in the inner detector might impact the performance of the pixel detector and silicon strip tracker and reduce the muon tracking efficiency.

Most tracks in PbPb collisions originate from a single primary vertex, in contrast to high-luminosity pp collisions, where the tracks originate from vertices with different positions along the

2024 JINST 19 P09012

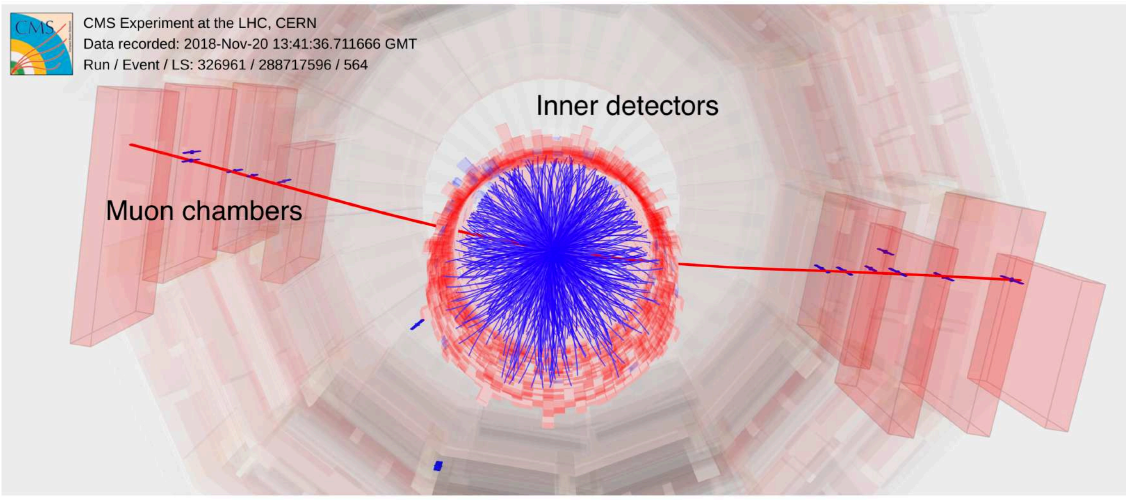

Figure 3. Dimuon event from a PbPb collision in the CMS detector. Particles reconstructed in the inner tracker are colored blue; two muons from a Z boson candidate are colored red. See text for details.

beam line. The separation between vertices in pp collisions is used to mitigate the effect of pileup on the reconstruction. The single-vertex origin, together with higher multiplicity, are factors that were addressed in the reconstruction of PbPb events.

4.1 Muon triggers in the heavy ion environment

An important component of all muon measurements involves an efficient selection of collision events that contain muons. The real-time (online) muon reconstruction algorithms in heavy ion collisions are generally identical to those used in pp collisions. This is true for both the L1 trigger and the HLT. There are three different types of muons defined in the CMS trigger system, commonly referred to as L1, L2, and L3 muons. An L1 muon is identified by the hardware-based L1 trigger system using solely the muon detectors. The L2 and L3 muons are defined within the HLT: an L2 muon uses only information from the muon detectors, while an L3 muon additionally matches the track from the muon detectors to a track from the inner tracker. In each subsequent level, the momentum resolution and purity (defined in section 7.2) are improved, as studied in ref. [27].

The heavy ion runs are characterized by a much smaller instantaneous luminosity and interaction rate when compared with 13 TeV pp runs. The lower rate allows the use of looser trigger requirements in PbPb: lower p_{T} thresholds are used for muons, as well as lower quality requirements (e.g., no isolation criterion). Relaxing the requirements benefits the physics program that is based on heavy ion muon data, focusing on open heavy flavor, quarkonium, and electroweak boson production; particularly by increasing the quarkonium acceptance in the low-p_{T} part of the spectrum.

Two main triggers used in analyses involving muons are studied in this paper: a high-p_{T} single-muon trigger (designed for the measurements of electroweak bosons and top quarks), and a low-p_{T} double-muon trigger (for quarkonia and B mesons). Each of these triggers is described in more detail in sections 7.2 (high-p_{T} single-muon) and 8.2 (low-p_{T} double-muon). To quantify the performance of these triggers, we collected an independent sample of muons using monitoring triggers. The monitoring triggers were single-muon HLT triggers with varying p_{T} thresholds. The single-muon triggers were used because any muon that satisfies the trigger can be used as a tag, and any other

2024 JINST 19 P09012

muon in the event can be used as a probe, since it has no trigger requirement imposed on it. Thus, the monitoring triggers allowed us to collect a muon-rich sample that is minimally biased for the purpose of the tag-and-probe analyses.

5 Extraction of efficiencies

We express the total muon efficiency, ϵ_μ, as the product of three contributions: muon reconstruction efficiency ($\epsilon_{\text{reco|track}}$), identification efficiency ($\epsilon_{\text{ID|reco}}$), and triggering efficiency ($\epsilon_{\text{trig|ID}}$), such that:

$$\epsilon_\mu = \epsilon_{\text{reco|track}}\, \epsilon_{\text{ID|reco}}\, \epsilon_{\text{trig|ID}} \tag{5.1}$$

Each efficiency is calculated as the fraction of muons that pass the specific selection in eq. (5.1). The numerator in one step (e.g., muon passing the identification requirements) is used as a denominator in the next step (e.g., trigger), ensuring the factorization of the total efficiency. Therefore, the particular efficiencies are relative rather than absolute, showing the efficiency with respect to the previous step. In the case of the first step, $\epsilon_{\text{reco|track}}$, the denominator consists of tracks from the silicon tracker with minimal quality requirements, such that very few genuine muons are removed from the denominator. The efficiency related to finding the tracks in the inner tracker, ϵ_{track}, is investigated separately (see ref. [28], where ϵ_{track} is obtained for pp collisions using simulated single muons). For purposes of this paper it is not included in eq. (5.1). The variable $\epsilon_{\text{reco|track}}$ quantifies the reconstruction efficiency in the outer muon detectors and the efficiency of matching tracks from the silicon tracker to tracks from the muon detectors.

The muon efficiencies are calculated using the data-driven tag-and-probe method (an example of its use in CMS is presented in ref. [4]). First, we select events where a resonance, such as the J/ψ meson or the Z boson, was likely to have decayed into a muon pair, producing a distinct peak in the dimuon invariant mass distribution. In these events, the 'tag' muon is a muon that satisfies strict requirements, such that its probability of being a genuine muon is as high as possible. Once we have 'tagged' a muon with a high level of confidence, we pair it with a second muon picked with much more relaxed requirements, in order to 'probe' its properties. The requirements placed on the probe muon define the denominator of the efficiency and are thus chosen in accordance with the factorization in eq. (5.1). With one tag muon and one probe muon, we construct tag-probe pairs and obtain an invariant mass distribution. The left panel of figure 4 shows an example of this invariant mass distribution, in which we have reconstructed the Z boson mass peak to study the probe muons in the kinematic region of $15 < p_{\text{T}} < 200\,\text{GeV}$. Next, we apply to the probes the selection criteria that we want to study. The subset of muons that pass these selection criteria are labeled 'passing probes', which then define the numerator in the efficiency. Those muons that fail the selection in question are dubbed 'failing probes'. We construct invariant mass distributions for each, seen in the middle panel of figure 4 for passing probes, and in the right panel for failing probes.

We perform a simultaneous fit to passing and failing distributions to measure the efficiency. The simultaneous fit includes both a signal and a background component for each invariant mass distribution. Only contributions from the signal peaks are considered in the efficiency calculation. The signal yields from the fit are denoted as N_{total}, N_{pass}, and N_{fail} for total, passing, and failing probes, respectively. Since the sum of passing and failing probes equals the total of all probe muons contained

2024 JINST 19 P09012

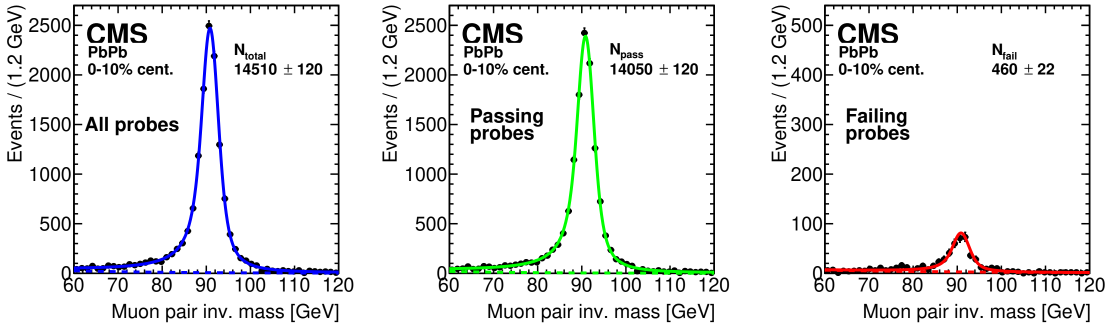

Figure 4. Example of a fit to the data in PbPb collisions. The three panels show invariant mass distributions of the tag-and-probe pairs in central 0–10% collisions fitted with the sum of signal and background components. Left panel: total spectrum. Middle panel: spectrum for pairs where the probe passed the muon identification selection. Right panel: spectrum for muon pairs where the probe failed the selection. The vertical scale of the failing probes is enhanced by a factor of 5 compared with the other panels for visibility. The yields displayed in the legends of the figures correspond to the Z boson signal as extracted from the fitting procedure described in the text. The efficiency is retrieved directly from the simultaneous fit and in this particular case is $\epsilon = 0.968 \pm 0.002$.

in the signal peak, the corresponding yields are related as follows:

$$N_{\text{pass}} = \epsilon\, N_{\text{total}} \tag{5.2}$$

$$N_{\text{fail}} = (1 - \epsilon)\, N_{\text{total}} \tag{5.3}$$

We can obtain the efficiency, ϵ, by appropriately including it as a parameter in the simultaneous fit. The statistical uncertainty of the efficiency is calculated directly in the fitting procedure, and takes into account the uncertainties in the parameters that describe both the signal and the background. The systematic uncertainty is obtained by choosing alternative functions to describe the signal and background shapes and by varying the fitting range. The systematic uncertainty obtained from the signal-shape variation is typically <0.1% when binning the data as a function of N_{tracks}. The corresponding uncertainty for the background-shape variation is <0.4%, and for the fitting-range variation it is <0.4%. When studying the uncertainty in a specific kinematic region, the uncertainty in a few cases can reach up to a few percent. The comparisons among the different collision systems are not significantly affected by the systematic uncertainties, given their small size. Furthermore, we analyzed the fits such as those in figure 4 across all collision systems using the same signal shape and fitting ranges to minimize the effects of the signal and mass range selection on the efficiency comparisons. The remaining source of systematic uncertainty, the background shape, can be different due to the varying amounts of combinatorial background for each collision system. Overall, the effects of systematic uncertainty are smaller than the size of the statistical uncertainty in the data, and are therefore not shown in the figures. For the MC simulations, the sizes of the statistical uncertainties are generally smaller than the symbols.

Events with muon pairs from decays of Z boson and J/ψ resonances are used to measure the efficiencies. Because of the different mass of these particles, the decay muons have different p_{T} spectra, allowing for the study of efficiencies in different kinematic regimes. In particular, muons from the Z boson peak are used in the p_{T} range 15–200 GeV, whereas the muons from the J/ψ peak are used for studies in the low-p_T range 0.8–25 GeV. The efficiency corrections obtained from the tag-and-probe method are then applied to each muon that enters a CMS analysis, under the assumption that the muon detection efficiency is independent of the type of parent particle that produces the decay muon. This assumption holds when the two decay muons are sufficiently separated in (η, ϕ), where ϕ is the azimuthal angle in radians, such that the detection of the one muon is independent of the detection of the other. The efficiencies can also be used for muons that come from a secondary vertex (such as those from nonprompt J/ψ decays) as long as the analysis applies selections that are consistent with those used to derive the efficiencies. With these considerations, the tag-and-probe method is used in section 6 for studying the muon reconstruction efficiency, and in sections 7 and 8 for identification and trigger efficiencies using the Z and J/ψ resonances, respectively.

6 Muon reconstruction

The algorithms for offline muon reconstruction for 13 TeV pp data in Run 2 are documented in ref. [29]. The same algorithms are used for the reconstruction of pPb data, as well as of pp reference data for heavy ions. The algorithms used in 2018 PbPb data taking were based on the pp algorithms with only minor customizations related primarily to the track selection. The customized pp algorithms worked in the PbPb environment, despite the large increase in detector occupancy, because the addition of a fourth layer to the pixel detector, as mentioned in section 3.1. The fourth layer allowed the use of higher quality four-hit seeds for the first tracking step, which significantly reduced the rate of spurious combinations of hits and thus the processing time needed per event.

The CMS muon reconstruction starts by creating 'tracker tracks', which are tracks reconstructed using only information from the inner tracker; and 'standalone muons', which are reconstructed only from the muon system. Two approaches are then used [4, 30]:

- *Global muon reconstruction (outside-in)*: reconstruction starts with a standalone muon, which is then used to look for possible track matches in the inner tracker. A 'global muon' is then obtained from fitting the combined hits of the two track components.

- *Tracker muon reconstruction (inside-out)*: a complementary approach starts with all tracker tracks with $p_T > 0.5$ GeV ($p_T > 0.8$ GeV for PbPb collisions) and momentum $p > 2.5$ GeV. These are extrapolated to the muon system, and if at least one matching muon segment is found, the track is qualified as a 'tracker muon'. The principal advantage of this approach is that it reconstructs lower-momentum muons more efficiently than the outside-in method. The drawback is that the algorithm starts with a much higher number of tracks, as the occupancy in the tracker is much larger than in the muon detectors.

Almost all of the muons (≈99%) in the detector's kinematic range are successfully reconstructed as global or tracker muons [4].

Reconstructed muons are used as input into the CMS particle-flow (PF) algorithm [31], which combines information from all CMS subdetectors to identify and reconstruct all individual particles for each event, including electrons, photons, neutral hadrons, charged hadrons, and muons. For muons, the PF algorithm applies a set of selection criteria to candidates reconstructed with the standalone, global, or tracker muon algorithms [29].

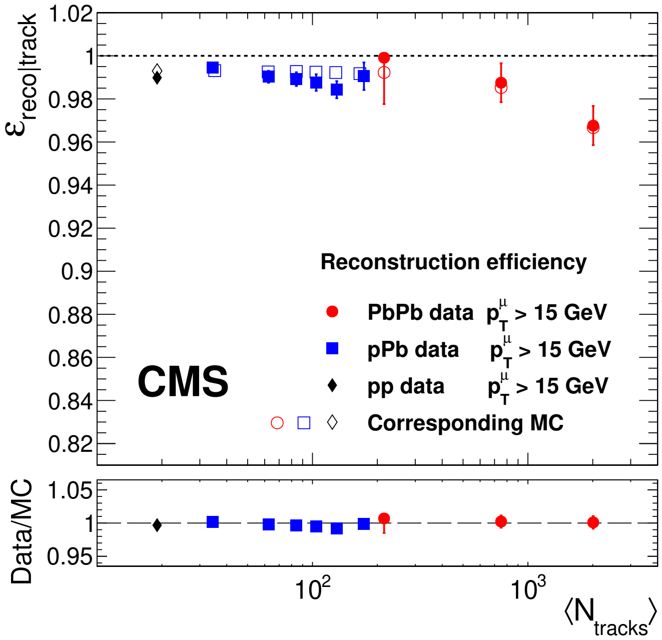

Figure 5. Muon reconstruction efficiency (defined as the probability that a given muon that produced a tracker track will be reconstructed as both a global and a PF muon) plotted as a function of the number of tracks in pp, pPb, and PbPb collisions. Open symbols are the MC results corresponding to each data set. Lower panel shows the ratio between data and MC simulation. Only statistical uncertainties are shown.

Figure 5 shows the reconstruction efficiency $\epsilon_{reco|track}$ for muons with $p_T > 15$ GeV in pp, pPb, and PbPb collisions as a function of N_{tracks}, obtained from fits to the Z boson resonance. In this case, probes are defined as any track reconstructed in the inner tracking system with a set of basic quality requirements (at least one hit in the pixel detector and a signal in at least six tracker layers). The passing probe satisfies both global-muon and PF-muon requirements. The reconstruction has high efficiency ($\gtrsim$97%) across the range of occupancies, although it exhibits a minor deterioration towards the most central PbPb collisions, both in collision data (filled points) and MC simulations (open points). We note that the track multiplicity increases by about 2 orders of magnitude from pp to central PbPb collisions, while the efficiency drops only 2 percentage points. To obtain the tracking efficiency in the inner tracker specifically, which can be added to eq. (5.1) to account for the tracking efficiency factor, ϵ_{track}, we can use a standalone muon as a probe and a corresponding inner track as a passing probe. From this complementary approach (not shown) we find that the inner tracking efficiency is high ($\gtrsim$97%) even in the large multiplicity environment. The results indicate that the CMS muon reconstruction is robust against large increases in the inner detector occupancy.

7 Studies in the Z boson kinematic region

The dimuon decay of the Z resonance is used to study the efficiencies for muons in the kinematic range $15 < p_T < 200$ GeV. The p_T range is bounded by the kinematics of the Z boson decay muons and by the number of such decays in the studied data set. The efficiencies obtained from the Z boson peak region have been used for several high-momentum analyses in pPb and PbPb collisions, such

Table 3. Overview of muon identification and triggers used in the Z boson kinematic region (e.g., Z, W, and t analyses) and in the J/ψ kinematic region (e.g., J/ψ and Y analyses). A description of muon identification and triggers is given in the text.

Region	Collision system	Muon ID	Trigger
Z	pp/pPb/PbPb	Tight	Single muon; $p_T > 12$ GeV; decision at HLT
	pp	Hybrid-soft	Double muon; no p_T requirement; decision at L1
J/ψ	pPb	Soft	Double muon; no p_T requirement; decision at L1
	PbPb	Hybrid-soft	Double muon; p_T, mass, and ΔR requirements; decision at HLT

as the studies of Z boson [32, 33], W boson [34], and $t\bar{t}$ production via $t \to W^+b \to \mu^+\nu b$ [35]. Table 3 summarizes the settings that are commonly used in CMS analyses with muons in the Z boson kinematic region, and in the J/ψ kinematic region (section 8). Following eq. (5.1), muon identification efficiency in the Z boson kinematic range starts with the set of muons that satisfy both the global and the PF muon requirement ($\epsilon_{\mathrm{ID|reco}}$ denominator). This is done because the set constitutes the passing probes in the previous step ($\epsilon_{\mathrm{reco|track}}$ numerator). Section 7.1 explains the muon ID and section 7.2 discusses the trigger.

7.1 Muon identification efficiency

The majority of the CMS heavy ion results that are using muons in the 15–200 GeV p_T range apply the 'tight-muon' selection, which is identical to that used in pp analyses [4]. The selection is as follows:

- Global muon and PF muon: The muon is reconstructed as both a global and a PF muon, as outlined in section 6.
- Fit χ^2/dof < 10 and number of muon hits >0: The global muon fit must be of good quality to reduce the number of muons from nonprompt hadron decays and the number of hadrons that traverse the inner detectors and pass through the magnet, reaching the muon chambers (hadronic punch-through). The selection places a limit on the fit χ^2/dof (where dof stands for degrees of freedom) and requires at least one muon detector hit included in the fit.
- Number of matched muon stations ≥ 2: At least two muon stations must be matched to the muon to further reduce hadronic punch-through.
- Number of pixel hits >0 and number of strip layers >5: To further improve the muon track quality and provide a good p_T measurement, minimal numbers of pixel hits and strip layers with hits are required.
- $D_{xy} < 0.2$ cm and $D_z < 0.5$ cm: An upper limit on the distance of closest approach between the primary vertex and the muon track in the transverse plane, D_{xy}, is used. This requirement selects muons from prompt decays and reduces contributions from cosmic rays and from nonprompt decays of hadrons. The corresponding limit in the longitudinal direction D_z is larger, due to coarser resolution of the tracker in the z coordinate.

Figure 6 displays the N_{tracks} dependence of the tight muon ID efficiency. The efficiencies in pp, pPb, and PbPb collisions are in good agreement with each other. The values are consistent with a constant in the full range of N_{tracks} reached in pp and pPb collisions, but exhibit a minor drop for the

2024 JINST 19 P09012

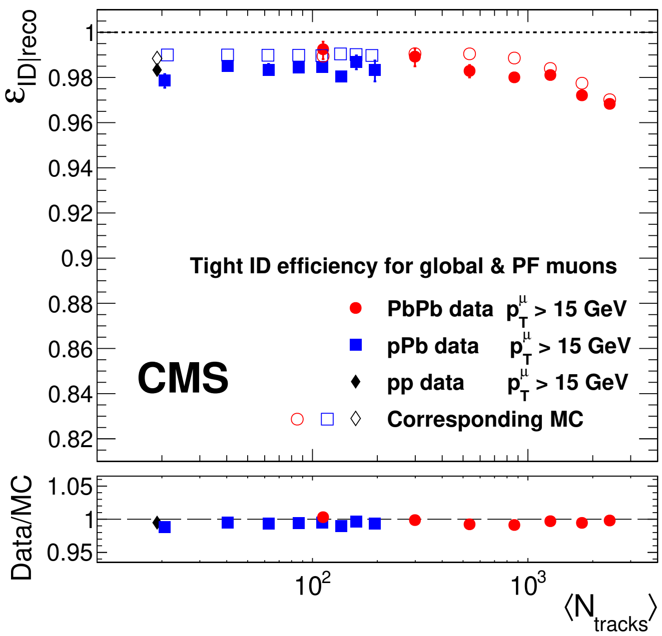

Figure 6. Tight ID efficiency for global and PF muons as a function of the number of tracks in pp, pPb, and PbPb collisions. Open symbols are the MC results corresponding to each data set. Lower panel shows the ratio between data and MC simulation. Only statistical uncertainties are shown.

central PbPb collisions. Even with track multiplicity over 2000, the efficiency only falls to about 96%. Figure 7 shows the kinematic dependence. The efficiency in PbPb collisions is comparable with that from lower multiplicity collisions in most of the studied kinematic range. However, the PbPb efficiency is 1–2% lower in the region of $15 < p_T \lesssim 40$ GeV and in the barrel-endcap overlap region ($0.9 < |\eta| < 1.2$). This loss of efficiency is caused primarily by the tight ID requirement of at least two matched muon stations. This requirement is met by fewer muons when the occupancy is high, which is the reason for the slight efficiency decrease in central collisions seen in figure 6. The two-matched-stations requirement is also the primary cause for the small difference between the data and MC results in both figures 6 and 7. Even though the MC description of the tight muon identification slightly overestimates its efficiency, it captures all the trends visible in data.

7.2 Muon trigger efficiency and purity

The tag-and-probe method is used to measure the efficiency of both trigger levels (L1+HLT) combined. In all the collision systems, the HLT studied here is a single-muon trigger with a requirement of $p_T > 12$ GeV at the HLT. The L1 seed was tailored to the specific conditions of each data-taking run. In PbPb collisions, the seed has a p_T threshold of 3 GeV; in pp and pPb collisions only L1 muons with $p_T > 7$ GeV were considered by the HLT.

Figure 8 shows the trigger efficiency as a function of N_{tracks}. The probes for the trigger efficiency (denominator) are the tight muons; the passing probes (numerator) are those tight muons that also pass the trigger requirement, following the factorization scheme of eq. (5.1). The quantitative comparison among all three data sets is affected by the upgrades to the detector between each corresponding run. In addition, the 2018 PbPb data set is affected by the optimizations of the HLT that were done

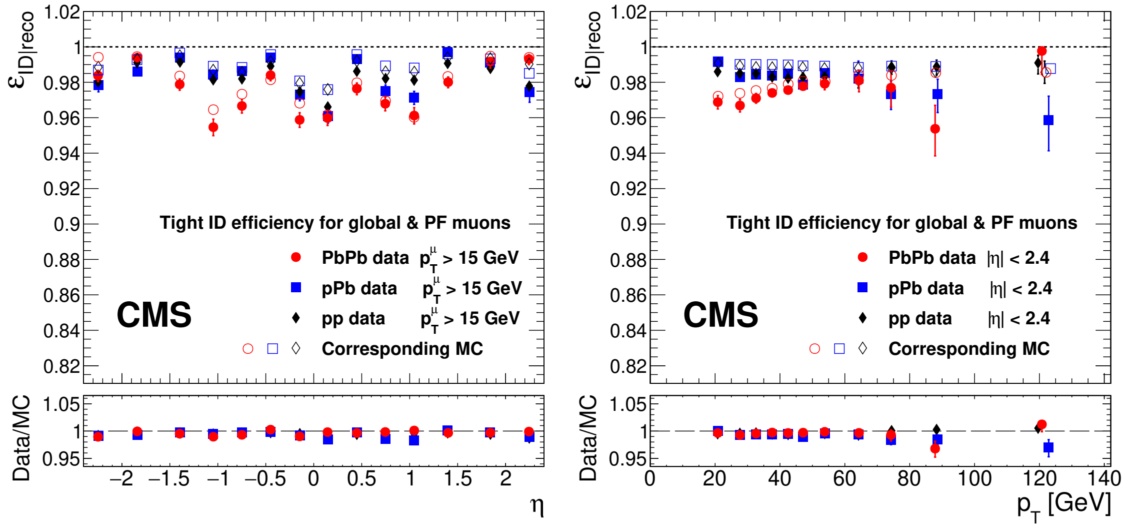

Figure 7. Tight ID efficiency as a function of η (left) and p_T (right) in pp, pPb, and PbPb collisions. The probe is both a global muon and a PF muon. Open symbols are the MC results corresponding to each data set. Lower panels show the ratio between data and MC simulation. Only statistical uncertainties are shown.

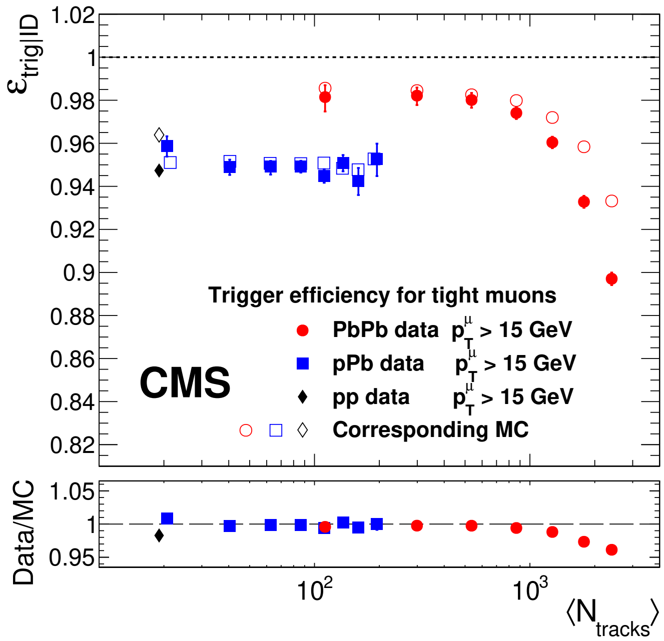

Figure 8. Trigger efficiency of tight muons as a function of the number of tracks. The trigger requires a single muon with p_T above 12 GeV. The efficiency is calculated for muons with $p_T > 15$ GeV to avoid threshold effects. Open symbols are the MC results corresponding to each data set. Lower panel shows the ratio between data and MC simulation. Only statistical uncertainties are shown. The significant increase in the trigger efficiency for the PbPb data set occurs because of detector upgrades and trigger optimizations prior to the 2018 data-taking period.

2024 JINST 19 P09012

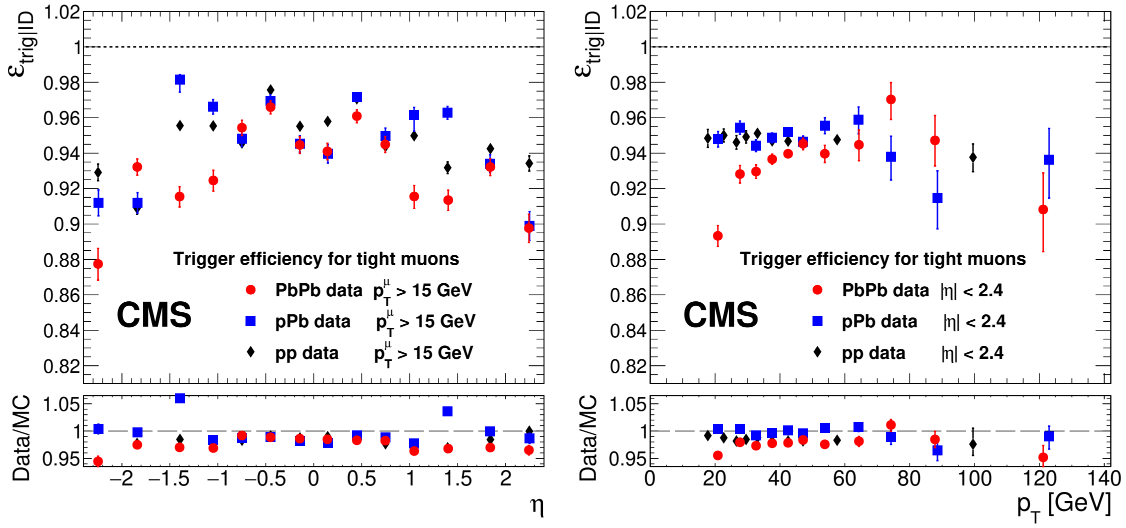

Figure 9. Trigger efficiency of tight muons as a function of η (left) and p_T (right) in pp, pPb, and PbPb collisions. Lower panels show the ratio between data and MC simulation (MC points are omitted in the upper panels for clarity). Only statistical uncertainties are shown.

between 2017 and 2018 [27]. The combination of the detector upgrades and trigger optimizations increased the overall efficiency in PbPb data when compared with the pp and pPb data taken in previous years, as seen by the efficiency shift from pPb to peripheral PbPb in the figure. With these changes taken into consideration, the efficiency is effectively flat in the N_{tracks} range covered by pp and pPb collisions, but begins to decline in more central PbPb events after the number of tracks in the detector surpasses several hundred. This drop is more pronounced for the trigger efficiency than was observed for muon ID (figure 6), suggesting that the former is more sensitive to detector occupancy than the latter. The MC simulations (open symbols) describe the general trends in data fairly well, however the trigger simulation for PbPb collisions overestimates the efficiency for central events. Figure 9 shows the efficiency dependence on the muon kinematics. We observe similar trends to those for the ID efficiency: the trigger in PbPb collisions is less efficient in the intermediate pseudorapidity region ($1.0 < |\eta| < 1.6$). While the efficiency stays mostly flat as a function of p_T in pp and pPb events, it decreases towards low p_T in PbPb events. In both pp and pPb collisions the trigger efficiency reaches a plateau at ≈95% for muons with $p_T > 20$ GeV. The PbPb muons at 20 GeV have a trigger efficiency of about 89%; the efficiency rises until $p_T \approx 40$ GeV, at which point it reaches a plateau. From the data to MC simulation ratio, we can infer that the simulation captures the trends fairly well, but overestimates the efficiency in PbPb events for muons with $p_T \lesssim 70$ GeV. The η-dependence of the data/simulation ratio for PbPb collisions is reasonably flat; the overall shift in the results of the simulation is caused by the overestimation in the high-N_{tracks} low-p_T region that was previously noted.

The trigger purity, which quantifies the capability to avoid triggering on particles that are not genuine prompt muons, is an important component for the determination of the trigger rate. We explore the purity of the three online muon definitions described in section 4.1 — L1, L2, and L3 — to illustrate improvements in purity at each subsequent trigger stage. We define the purity as a ratio of the numbers of muons in the two samples. The sample in the denominator is the set of online muons passing the relevant trigger step and having an online $p_T > 15$ GeV requirement in

2024 JINST 19 P09012

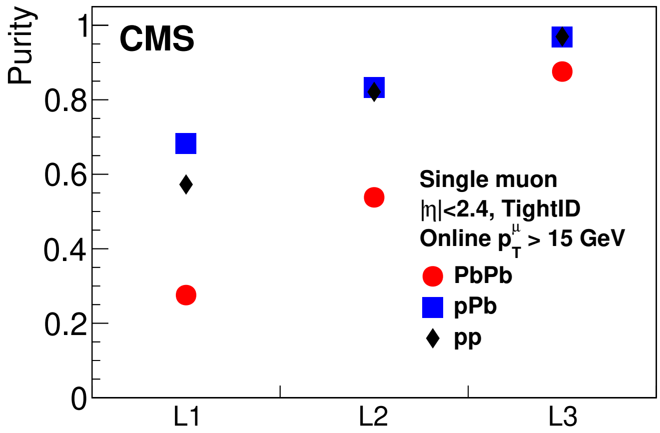

Figure 10. Purity for the L1, L2, and L3 trigger steps, compared among pp, pPb, and PbPb collisions. The online muon must have $p_T > 15$ GeV and the offline muon matched to it must pass the tight ID selection and have $|\eta| < 2.4$. Details of the purity definition are given in the text. Statistical uncertainties are smaller than the symbol sizes.

order to focus on muons from the Z boson decay. The numerator is meant to be genuine muons, which in our case are the subset of online muons consisting of those matched geometrically within $\Delta R \equiv \sqrt{(\Delta\phi)^2 + (\Delta\eta)^2} < 0.3$ (0.1 for L3) to an offline muon that must satisfy the tight ID requirement. Offline muons must have $|\eta| < 2.4$ without an additional p_T requirement. For our study, muons were collected with dimuon triggers that utilize L1/L2/L3 trigger selections. Although the exact values of the purity are dependent on the details of the trigger that was used to collect the muon sample, the study provides useful qualitative comparisons among the collision systems and trigger steps. The results of the purity study are shown in figure 10. The purity values in pp and pPb collisions are similar, whereas the purity in PbPb collisions is lower. The figure also illustrates how the purity improves in each successive and more complex trigger step, thus reducing the rate. Although the rate is reduced, the HLT maintains a very high efficiency, as seen earlier in figure 8. Backgrounds to the purity include primarily muons from long-lived hadron decays. For the L3 trigger, the background also includes muons where a track from the muon chambers is matched to one inner track online, but offline it is matched to a different track. This occurs more often in high multiplicity PbPb collisions.

8 Studies in the J/ψ kinematic region

The J/ψ resonance is used to derive the efficiencies for low-p_T muons. The acceptance at low-p_T is limited by the material in front of the muon stations [36] and by the strength of the CMS magnetic field. Figure 11 details the acceptance regions commonly used for the various collision systems. The green curves, with higher-p_T thresholds, pertain to analyses that use the most frequently employed muon trigger in heavy ion collisions. The red curves, with lower thresholds in p_T, are used for muon selection by those analyses that use only muon identification and do not use a dedicated muon trigger (e.g., they use a jet trigger or a minimum-bias trigger to collect their data samples). The existence of the two distinct acceptance regions in each collision system arises from the better low-p_T efficiency of muon identification compared with that of the muon trigger. The lower portion of table 3 summarizes muon

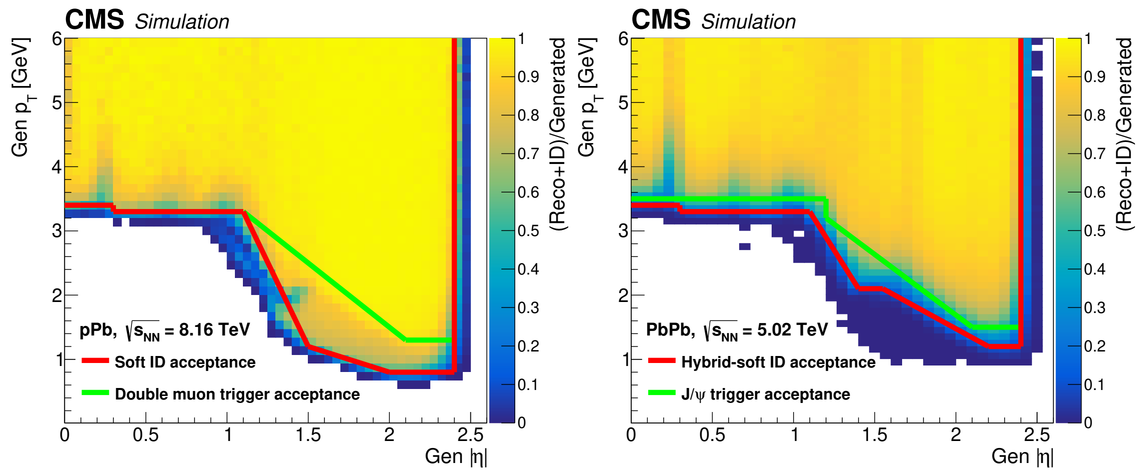

Figure 11. Regions of the CMS detector commonly used in the heavy ion muon analyses for pPb (left) and PbPb (right) collisions. For each panel, the combined reconstruction and identification efficiency for simulated muons is plotted as a function of generated muon $|\eta|$ and p_{T}. The lower-threshold curves (red) are for muon identification, and are used only by those analyses that do not use a dedicated muon trigger. The higher-threshold curves (green) are used by most analyses (those using the muon trigger information).

ID selections and triggers commonly used in the J/ψ kinematic region in the various collision systems. The muon ID selections are explored in section 8.1 and the triggers are discussed in section 8.2.

8.1 Muon identification efficiency

The 'soft muon' ID [4, 29] denotes a set of selection criteria that is commonly used within CMS for low-p_{T} muons. The selection has been further optimized for the heavy ion environment and the resulting selection is called 'hybrid-soft muon'. The hybrid-soft muon ID is used in PbPb analyses, as well as for pp reference data, and consists of the following requirements:

- Tracker muon and global muon: The muon is reconstructed as both a tracker and a global muon (defined in section 6) to reduce the misidentification rate.
- Number of pixel layers >0 and number of strip layers with hits >5: To further improve muon-track quality, we impose a minimum on the numbers of pixel layers and strip layers associated with the track.
- $D_{\mathrm{xy}} < 0.3$ cm and $D_{\mathrm{z}} < 20$ cm: An upper limit on the distance of closest approach between the event vertex and the muon track in the transverse plane, D_{xy}, selects muons from prompt decays, and reduces contributions from cosmic rays and from nonprompt hadron decays. The variable D_{z} is the corresponding longitudinal component of the distance of closest approach, and the requirement on D_{z} is very loose.

The soft muon ID differs from the hybrid-soft ID by having a high-purity requirement [37] applied to the tracker tracks, instead of requiring the muon to be a global muon. The soft muon ID is used in pPb and other pp collisions in general, as it allows reaching lower-p_{T} than does hybrid-soft ID. The soft muon ID is not ideal for PbPb collision data, since the high-purity requirement has a low efficiency in the central collisions.

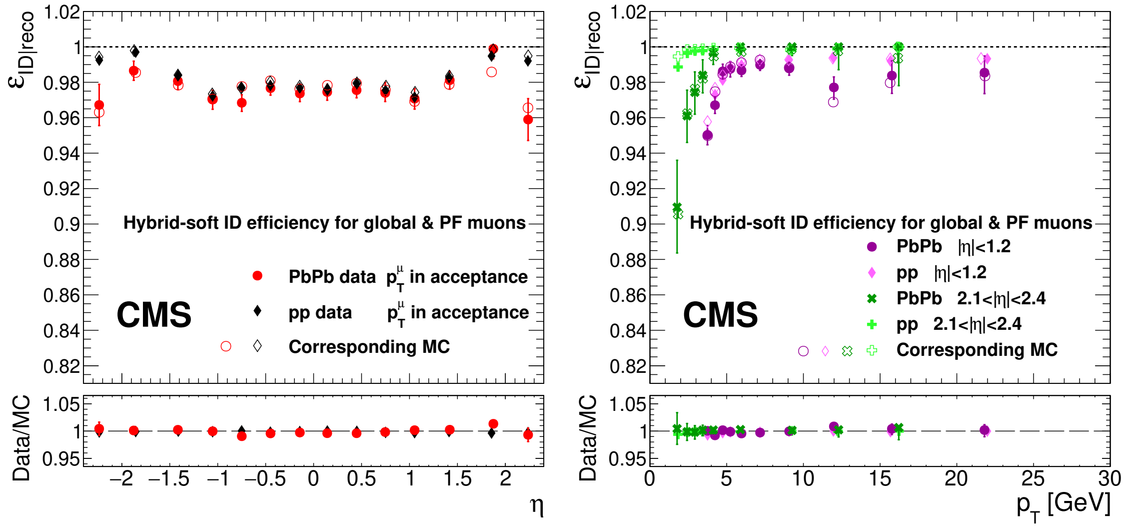

Figure 12. Hybrid-soft ID efficiency for global muons as a function of η (left) and p_T (right) in pp and PbPb collisions. The muons are restricted in acceptance as shown by the red line in the right panel of figure 11. Lower panels show the ratio between data and MC simulation. Only statistical uncertainties are shown.

Figure 12 shows the pseudorapidity and p_T dependence of the efficiency of the hybrid-soft selection. The kinematic reach at low p_T is better in the endcap region (as seen in figure 11). The efficiency is comparable between the pp and PbPb collisions, except for the region of $|\eta| > 2$ and $p_T < 5$ GeV, where the occupancy in the tracker is the highest. We found that the drop occurs primarily in central PbPb events (not shown), in which the high number of tracks in the tracker leads to a decrease in matching efficiency with the standalone muons. This trend is well-described by the MC simulations (open points), indicating that they successfully model this behavior.

8.2 Muon triggers

The muon trigger used for quarkonia (e.g., J/ψ and Υ mesons) studies in pPb and for reference pp data sets is as loose as possible: a double-muon trigger at L1. It simply required two tracks in the muon system, with only very loose quality requirements and no explicit p_T threshold. The trigger decision is taken at L1 with no further filtering at the HLT stage. In PbPb collisions, the rate of this double-muon trigger at L1 was above the acceptable limit, so that additional quality requirements had to be placed at the HLT level to reduce the rate. One of the two muons was required to be an L2 muon; the other was required to be an L3 muon. This was done as a compromise between reducing the rate and keeping the efficiency as high as possible for low-p_T quarkonia. Two main HLT paths were used: one for charmonia and one for bottomonia. The charmonia path required the invariant mass of the dimuon to be within 1 and 5 GeV, and required a $\Delta R < 3.5$ between the two muons to suppress uncorrelated muons. The bottomonia path required a minimum mass of 7 GeV to cover the bottomonia mass region around 9.4–10.5 GeV, and minimum p_T requirements of 2.0 GeV for the L2 muon and 2.5 GeV for the L3 muon. Both triggers required that the muons in the pair have opposite charge. To complement the two main HLT trigger paths, centrality-gated triggers were used to select peripheral events, which have the smallest occupancy in PbPb collisions. Therefore, the data-stream size was able to be kept sufficiently low to satisfy bandwidth and storage limitations. The differences among the triggers used in pp, pPb, and PbPb collisions preclude meaningful comparisons of the trigger efficiency.

9 Mass resolution and scale

The masses of the Z boson and the J/ψ meson are well known from other results [38]. Measuring these particles via their dimuon decay can provide additional information about the muon reconstruction. The dimuon mass resolution provides a suitable window into the precision of the momentum measurement; the mean value of the mass peak is sensitive to the momentum scale of the detector. The momentum calibration procedure for our data sets is described in ref. [21]. The mass resolution is obtained from the width of the fitted dimuon resonance. We apply the same selection as we did for the trigger-efficiency evaluation, described in sections 7 and 8 for each corresponding resonance. To study the absolute scale of the momentum calibration, we plot the reconstructed mass of the resonance obtained from the fit, m_{fit}, scaled by the world-average mass obtained by the Particle Data Group (PDG), m_{PDG} [38]. Since measurements of particle masses using heavy ion data are rare, a small bias in the momentum scale has had little effect on the success of the overall program. In contrast, heavy-ion measurements are more sensitive to momentum resolution. For example, a degraded resolution would impact the signal-to-background ratio for resonances.

For the Z boson, the signal peak is described by a Breit–Wigner (BW) function convolved with a Crystal Ball (CB) function. The CB function consists of a Gaussian peak with a power-law tail grafted onto the lower-valued side, such that the function and its derivative are continuous [39]. In this case, the reconstructed mass, m_{fit}, is a common parameter between the CB and the BW functions that is both the mean of the Gaussian core of the CB function and the location parameter of the BW function. The width of the BW function is fixed to the natural width of the Z boson ($\Gamma_Z \approx 2.5\,\mathrm{GeV}$). The Gaussian width of the CB function, σ_{CB}, is a free parameter in the fit and summarizes our information about the muon resolution in the detector. We plot the parameter σ_{CB} divided by the Z boson PDG mass, m_{PDG}.

For the J/ψ meson, the BW function is not used because the natural width is negligible. Instead, the signal is described by a sum of a CB and a Gaussian function. In this case, the reconstructed mass, m_{fit}, is a mean common to the Gaussian core of the CB and to the additional Gaussian function. The two Gaussian width parameters of the signal function are kept distinct to account for the varying resolution in the barrel and endcap regions of the detector. To estimate the mass resolution of the J/ψ peak, we use the average of these two Gaussian widths, weighted by the amount of signal contained in each of the two functions. The extracted width is then divided by the corresponding m_{PDG}.

The estimated mass resolution is plotted in figure 13 as a function of N_{tracks} for the Z boson (left) and the J/ψ meson (right). The resolution in both cases is consistent with a constant value, which indicates that the resolution is not affected by the level of occupancy in the tracker. The estimated mass scale is plotted in figure 14 as a function of N_{tracks} for the Z boson (left) and the J/ψ meson (right). The reconstructed mass is lower than the true mass for both particles, but this scaling is consistent across the different collision systems and for all values of N_{tracks}, indicating that the momentum scale is accurate to approximately 0.3% and is unaffected by the level of occupancy in the tracker or the data-taking year. A change in the mass scale of this order does not generally affect heavy ion measurements, but there are cases (e.g., ref. [40]) in which such a change can be indicative of interesting physics.

The mass resolution and mass scale versus dimuon rapidity, $y^{\mu\mu}$, are shown in figures 15 and 16, respectively. The resolution varies significantly with rapidity due to the varying angle between the magnetic field $\vec{B}$ and the particle velocity $\vec{v}$. At forward rapidity, where $\vec{v}$ and $\vec{B}$ are almost collinear, a smaller Lorentz force reduces the magnetic bending. The resulting smaller sagitta leads to a greater uncertainty in the momentum measurement. Since the resolution is not constant, for signal description

2024 JINST 19 P09012

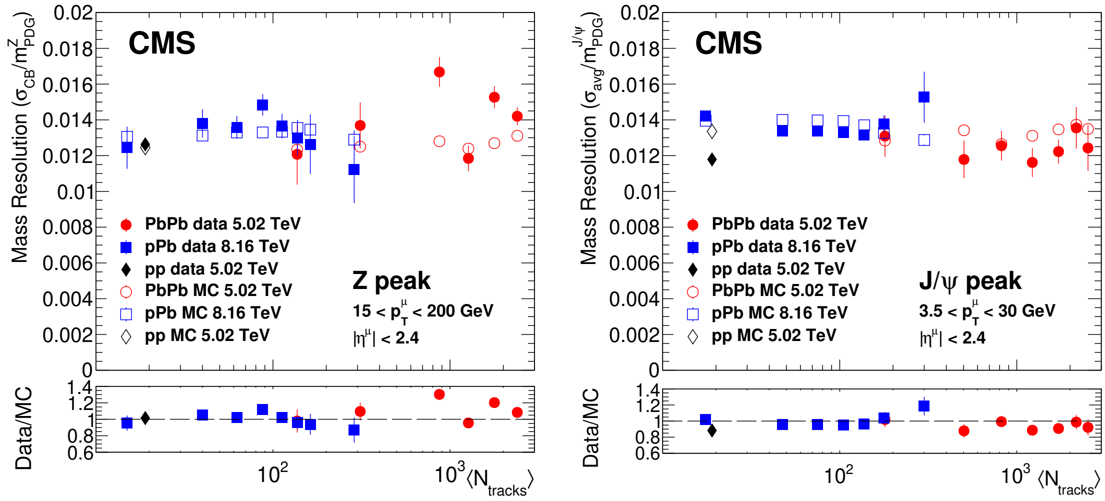

Figure 13. Mass resolution at the Z boson peak (left) and the J/ψ peak (right) as a function of the number of tracks from MC simulations (open points) and collision data (filled points) in pp, pPb, and PbPb collisions. The mass resolution is scaled by the world-average mass m_{PDG}. Lower panels show the ratio between data and MC simulation. Only statistical uncertainties are shown.

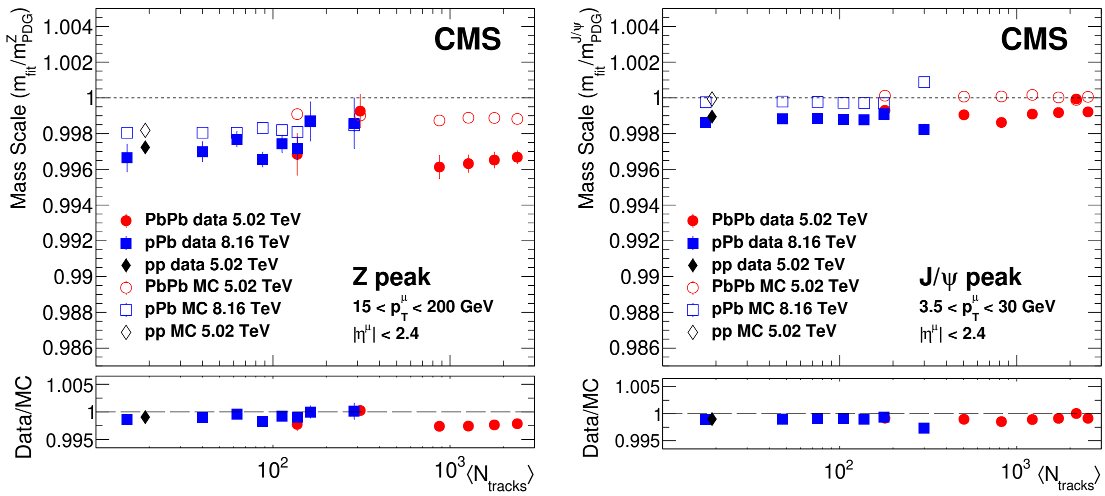

Figure 14. Mass scale at the Z boson peak (left) and the J/ψ peak (right) as a function of the number of tracks from MC simulations (open points) and collision data (filled points) in pp, pPb, and PbPb collisions, calculated as the measured mass m_{fit} divided by the world-average mass m_{PDG}. Lower panels show the ratio between data and MC simulation. Only statistical uncertainties are shown.

we use the two distinct Gaussian parameters mentioned earlier. The mass scale decreases slightly with rapidity at the J/ψ peak in data but not in MC simulations. At the Z boson peak, the corresponding decrease is more prominent and is present in both data and MC simulations. In most rapidity bins, the mass scale values tend to be slightly reduced ($\approx$0.2%) in data when compared with the MC results. The results are consistent among the pp, pPb, and PbPb collision systems and display the same trends.

Previous estimates of mass resolution and mass scale were carried out on a pp data set at a center-of-mass energy $\sqrt{s} = 7$ TeV in 2010 [41]. A comparison of these results with our data is shown

2024 JINST 19 P09012

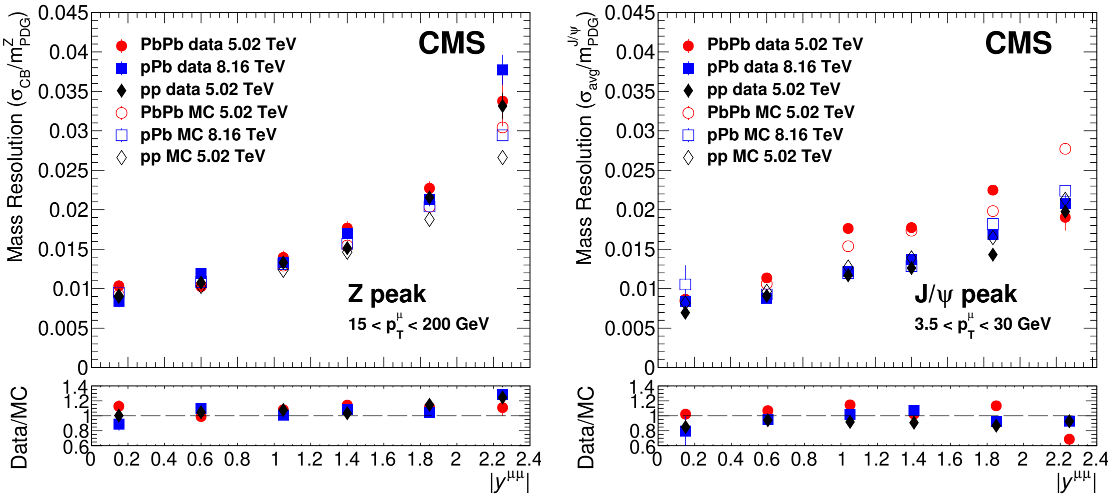

Figure 15. Mass resolution at the Z boson peak (left) and J/ψ peak (right) as a function of $|y^{\mu\mu}|$ from MC simulations (open points) and collision data (filled points) in pp, pPb, and PbPb collisions. The mass resolution is scaled by the world-average mass m_{PDG}. Lower panels show the ratio between data and MC simulation. Only statistical uncertainties are shown.

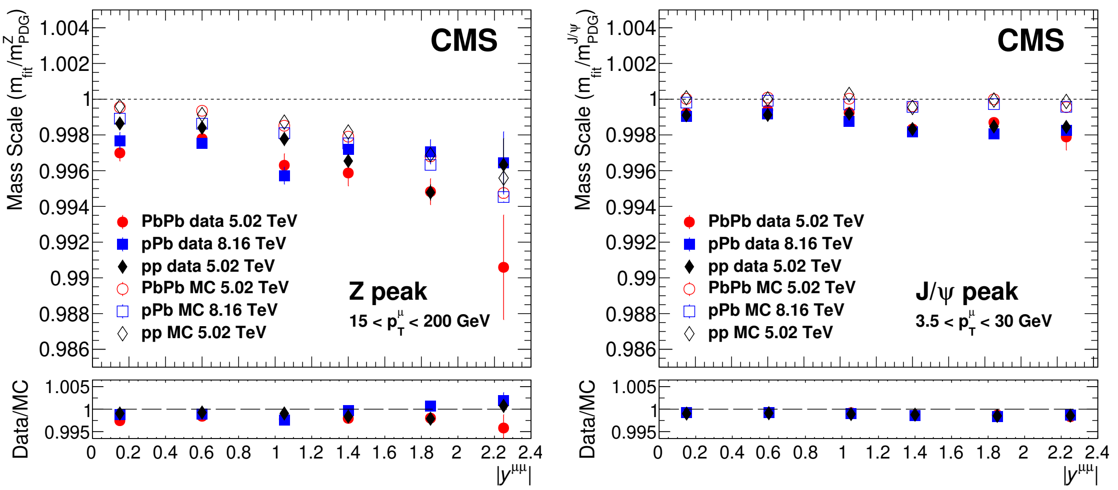

Figure 16. Mass scale at the Z boson peak (left) and the J/ψ peak (right) as a function of $|y^{\mu\mu}|$ from MC simulations (open points) and real data (filled points) in pp, pPb, and PbPb collisions, calculated as the measured mass m_{fit} divided by the PDG mass m_{PDG}. Lower panels show the ratio between data and MC simulation. Only statistical uncertainties are shown.

in figure 17 as a function of muon pseudorapidity $|\eta^\mu|$. In order to plot the mass resolution and scale versus pseudorapidity of a single muon, each value of the dimuon mass is entered twice in the distribution used to extract these results: once with the pseudorapidity of the first muon, and then with the pseudorapidity of the second muon. The results of ref. [41] were averaged over the forward and backward pseudorapidity bins. The comparison shows that the muon momentum scale and resolution have been remarkably stable throughout the lifetime of the experiment, indicating that the differences in center-of-mass energy, collision system, accelerator/detector conditions, and kinematic coverage have been successfully addressed by the CMS calibration and reconstruction frameworks.

2024 JINST 19 P09012

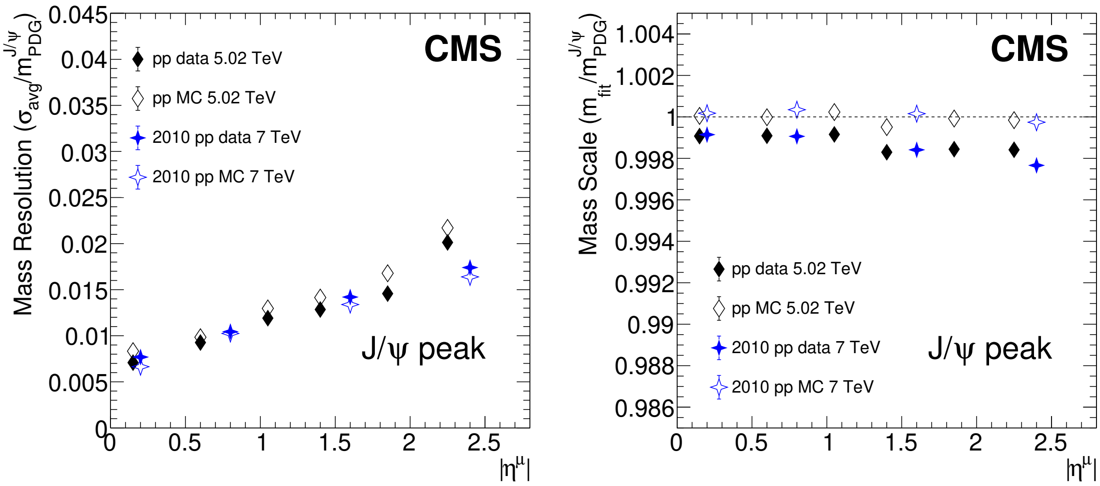

Figure 17. Mass resolution (left) and mass scale (right) versus the muon pseudorapidity $|\eta^{\mu}|$ at the J/ψ peak in pp collisions. The values are scaled by the world-average mass $m^{J/\psi}_{PDG}$. The filled points are collision data and the open points are MC simulations. Our results (black diamonds) are compared with measurements from a previous pp analysis done at $\sqrt{s} = 7$ TeV (blue crosses) [41]. Only statistical uncertainties are shown. See details in text.

10 Summary

We have presented efficiencies of muon reconstruction, identification, and triggering, as well as measurements of the dimuon mass scale and resolution of the CMS detector. The efficiencies were estimated using the data-driven tag-and-probe technique. Mass scale and resolution were derived through fits to the invariant mass spectra of J/ψ and Z boson resonances. We have extended previous studies of the muon performance in pp collisions to the heavy ion environment using PbPb data at $\sqrt{s_{NN}} = 5.02$ TeV and pPb data at $\sqrt{s_{NN}} = 8.16$ TeV. All the results were also measured in pp data at $\sqrt{s} = 5.02$ TeV for comparison across all collision systems as a function of the charged particle multiplicity, N_{tracks}.

The efficiencies are high (typically above 90%) in all cases, even at extremely high occupancy. In the low-p_T region, the muon-identification efficiency is comparable between pp and PbPb collisions, except in the region of highest occupancy at very low p_T (<5 GeV) and forward pseudorapidity ($|\eta| > 2$). This drop in efficiency is expected because the high number of tracks in the inner parts of the detector complicates the matching of tracks between the muon chambers and the tracker. In the high-p_T region, we observe a slight drop (1–2%) in the muon-identification efficiency in the most central PbPb events at multiplicities that are unattainable in pPb or pp events. A slight decrease (≈3%) in the reconstruction efficiency at high occupancies is also observed. Additionally, the trigger efficiency decreases in the most central PbPb events. A relative reduction of ≈8% in the trigger efficiency occurs between the lowest and highest N_{tracks} bins in PbPb collisions. This reduction is more pronounced than the corresponding decrease in the muon identification and reconstruction efficiencies, suggesting that the CMS single-muon trigger is more sensitive to detector occupancy. In most cases, the efficiencies calculated using Monte Carlo simulations capture the trends seen in data, indicating that the main features are contained in the detector simulation. In a few instances, the MC efficiencies overestimate those obtained from collision data (by up to 4 percentage points), highlighting the need for independent techniques of efficiency estimation based directly on collision data.

2024 JINST 19 P09012

The excellent muon performance of the CMS detector has made possible a robust muon and dimuon program in the heavy ion environment, leading to many muon-based measurements, where some examples include heavy quarkonia, heavy-flavor mesons [3, 42–52]; and electroweak bosons [32–34, 53, 54].

Acknowledgments

We congratulate our colleagues in the CERN accelerator departments for the excellent performance of the LHC and thank the technical and administrative staffs at CERN and at other CMS institutes for their contributions to the success of the CMS effort. In addition, we gratefully acknowledge the computing centers and personnel of the Worldwide LHC Computing Grid and other centers for delivering so effectively the computing infrastructure essential to our analyses. Finally, we acknowledge the enduring support for the construction and operation of the LHC, the CMS detector, and the supporting computing infrastructure provided by the following funding agencies: SC (Armenia), BMBWF and FWF (Austria); FNRS and FWO (Belgium); CNPq, CAPES, FAPERJ, FAPERGS, and FAPESP (Brazil); MES and BNSF (Bulgaria); CERN; CAS, MoST, and NSFC (China); MINCIENCIAS (Colombia); MSES and CSF (Croatia); RIF (Cyprus); SENESCYT (Ecuador); ERC PRG, RVTT3 and MoER TK202 (Estonia); Academy of Finland, MEC, and HIP (Finland); CEA and CNRS/IN2P3 (France); SRNSF (Georgia); BMBF, DFG, and HGF (Germany); GSRI (Greece); NKFIH (Hungary); DAE and DST (India); IPM (Iran); SFI (Ireland); INFN (Italy); MSIP and NRF (Republic of Korea); MES (Latvia); LMTLT (Lithuania); MOE and UM (Malaysia); BUAP, CINVESTAV, CONACYT, LNS, SEP, and UASLP-FAI (Mexico); MOS (Montenegro); MBIE (New Zealand); PAEC (Pakistan); MES and NSC (Poland); FCT (Portugal); MESTD (Serbia); MCIN/AEI and PCTI (Spain); MOSTR (Sri Lanka); Swiss Funding Agencies (Switzerland); MST (Taipei); MHESI and NSTDA (Thailand); TUBITAK and TENMAK (Turkey); NASU (Ukraine); STFC (United Kingdom); DOE and NSF (U.S.A.).

Individuals have received support from the Marie-Curie program and the European Research Council and Horizon 2020 Grant, contract Nos. 675440, 724704, 752730, 758316, 765710, 824093, 101115353, 101002207, and COST Action CA16108 (European Union); the Leventis Foundation; the Alfred P. Sloan Foundation; the Alexander von Humboldt Foundation; the Science Committee, project no. 22rl-037 (Armenia); the Belgian Federal Science Policy Office; the Fonds pour la Formation à la Recherche dans l'Industrie et dans l'Agriculture (FRIA-Belgium); the Agentschap voor Innovatie door Wetenschap en Technologie (IWT-Belgium); the F.R.S.-FNRS and FWO (Belgium) under the “Excellence of Science — EOS" — be.h project n. 30820817; the Beijing Municipal Science & Technology Commission, No. Z191100007219010 and Fundamental Research Funds for the Central Universities (China); the Ministry of Education, Youth and Sports (MEYS) of the Czech Republic; the Shota Rustaveli National Science Foundation, grant FR-22-985 (Georgia); the Deutsche Forschungsgemeinschaft (DFG), under Germany's Excellence Strategy — EXC 2121 “Quantum Universe" — 390833306, and under project number 400140256 — GRK2497; the Hellenic Foundation for Research and Innovation (HFRI), Project Number 2288 (Greece); the Hungarian Academy of Sciences, the New National Excellence Program — ÚNKP, the NKFIH research grants K 131991, K 133046, K 138136, K 143460, K 143477, K 146913, K 146914, K 147048, 2020-2.2.1-ED-2021-00181, and TKP2021-NKTA-64 (Hungary); the Council of Science and Industrial Research, India; ICSC — National Research Center for High Performance Computing, Big Data and Quantum Computing and FAIR — Future Artificial Intelligence Research, funded by the EU NexGeneration program (Italy); the

2024 JINST 19 P09012

Latvian Council of Science; the Ministry of Education and Science, project no. 2022/WK/14, and the National Science Center, contracts Opus 2021/41/B/ST2/01369 and 2021/43/B/ST2/01552 (Poland); the Fundação para a Ciência e a Tecnologia, grant CEECIND/01334/2018 (Portugal); the National Priorities Research Program by Qatar National Research Fund; MCIN/AEI/10.13039/501100011033, ERDF "a way of making Europe", and the Programa Estatal de Fomento de la Investigación Científica y Técnica de Excelencia María de Maeztu, grant MDM-2017-0765 and Programa Severo Ochoa del Principado de Asturias (Spain); the Chulalongkorn Academic into Its 2nd Century Project Advancement Project, and the National Science, Research and Innovation Fund via the Program Management Unit for Human Resources & Institutional Development, Research and Innovation, grant B37G660013 (Thailand); the Kavli Foundation; the Nvidia Corporation; the SuperMicro Corporation; the Welch Foundation, contract C-1845; and the Weston Havens Foundation (USA).

A Converting centrality to number of tracks

It is common in analyses of PbPb collisions to study observables in bins of centrality, whereas in pp and pPb collisions it is common to do so in bins of N_{tracks}. In order to compare the existing efficiency results in all three collision systems as a function of a common event activity variable, we converted the PbPb centrality bins to corresponding average values of N_{tracks}, which we label $\langle N_{\text{tracks}} \rangle$ in tables and figures. The N_{tracks} variable was chosen because it is suitable for studying occupancy-related effects.

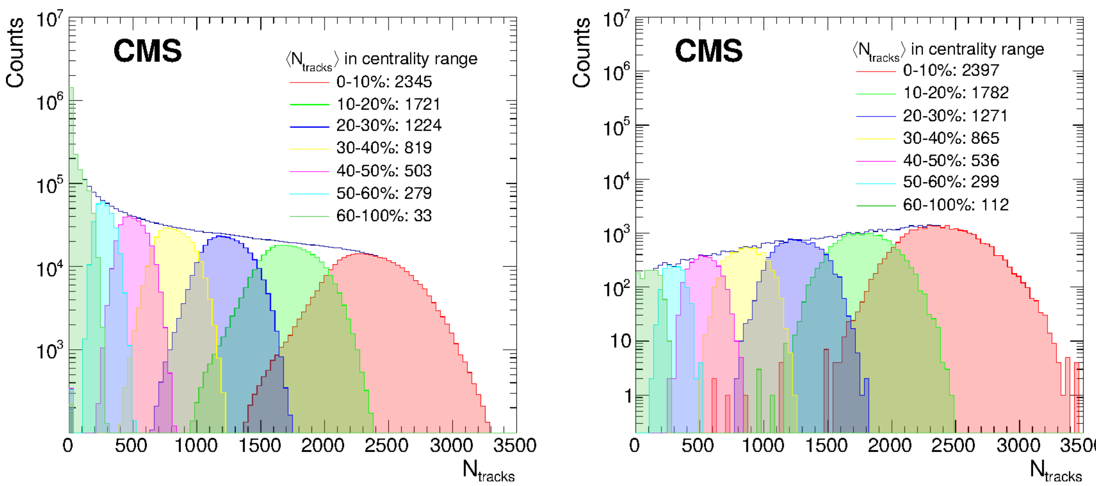

Figure 18. Distributions of N_{tracks} in the PbPb collisions for various ranges of centrality in a minimum-bias (left) and a muon-triggered (right) data set.

The conversion was done by plotting the distribution of N_{tracks} in the PbPb data set for each centrality bin and taking the mean of this distribution as the value of N_{tracks} for that efficiency datum point. Examples of the conversion procedure are shown in figure 18. The plot on the left was generated from a minimum-bias data set, which required that events must have a coincidence signal in both the positive-z and negative-z side of the HF. The plot on the right was from a muon-triggered data set, which required that events must have at least two muons passing various selection criteria common to dimuon analyses. Requiring two muons biases the average N_{tracks} toward higher values. The

2024 JINST 19 P09012

triggered data are used to translate centrality bins to N_{tracks} because they describe most accurately the occupancy conditions of the detector for our data samples.

References

[1] CMS collaboration, *Measurements of inclusive W and Z cross sections in pp collisions at* $\sqrt{s} = 7$ *TeV*, *JHEP* **01** (2011) 080 [arXiv:1012.2466].

[2] CMS collaboration, *Study of W boson production in pPb collisions at* $\sqrt{s_{\mathrm{NN}}} = 5.02$ *TeV*, *Phys. Lett. B* **750** (2015) 565 [arXiv:1503.05825].

[3] CMS collaboration, *Suppression of non-prompt* J/ψ*, prompt* J/ψ*, and Y(1S) in PbPb collisions at* $\sqrt{s_{NN}} = 2.76$ *TeV*, *JHEP* **05** (2012) 063 [arXiv:1201.5069].

[4] CMS collaboration, *Performance of CMS muon reconstruction in pp collision events at* $\sqrt{s} = 7$ *TeV*, 2012 *JINST* **7** P10002 [arXiv:1206.4071].

[5] CMS collaboration, *Performance of the reconstruction and identification of high-momentum muons in proton-proton collisions at* $\sqrt{s} = 13$ *TeV*, 2020 *JINST* **15** P02027 [arXiv:1912.03516].

[6] W. Busza, K. Rajagopal and W. van der Schee, *Heavy Ion Collisions: The Big Picture, and the Big Questions*, *Ann. Rev. Nucl. Part. Sci.* **68** (2018) 339 [arXiv:1802.04801].

[7] CMS collaboration, *Dependence on pseudorapidity and centrality of charged hadron production in PbPb collisions at a nucleon-nucleon centre-of-mass energy of 2.76 TeV*, *JHEP* **08** (2011) 141 [arXiv:1107.4800].

[8] CMS collaboration, *The CMS Experiment at the CERN LHC*, 2008 *JINST* **3** S08004.

[9] CMS collaboration, *The CMS trigger system*, 2017 *JINST* **12** P01020 [arXiv:1609.02366].

[10] CMS collaboration, *Performance of the CMS Level-1 trigger in proton-proton collisions at* $\sqrt{s} = 13$ *TeV*, 2020 *JINST* **15** P10017 [arXiv:2006.10165].

[11] GEANT4 collaboration, *GEANT4–a simulation toolkit*, *Nucl. Instrum. Meth. A* **506** (2003) 250.

[12] T. Sjöstrand et al., *An introduction to PYTHIA 8.2*, *Comput. Phys. Commun.* **191** (2015) 159 [arXiv:1410.3012].

[13] J. Alwall et al., *The automated computation of tree-level and next-to-leading order differential cross sections, and their matching to parton shower simulations*, *JHEP* **07** (2014) 079 [arXiv:1405.0301].

[14] P. Nason, *A New method for combining NLO QCD with shower Monte Carlo algorithms*, *JHEP* **11** (2004) 040 [hep-ph/0409146].

[15] S. Frixione, P. Nason and C. Oleari, *Matching NLO QCD computations with parton shower simulations: the POWHEG method*, *JHEP* **11** (2007) 070 [arXiv:0709.2092].

[16] S. Alioli, P. Nason, C. Oleari and E. Re, *A general framework for implementing NLO calculations in shower Monte Carlo programs: the POWHEG BOX*, *JHEP* **06** (2010) 043 [arXiv:1002.2581].

[17] S. Alioli, P. Nason, C. Oleari and E. Re, *NLO vector-boson production matched with shower in POWHEG*, *JHEP* **07** (2008) 060 [arXiv:0805.4802].

[18] T. Pierog et al., *EPOS LHC: Test of collective hadronization with data measured at the CERN Large Hadron Collider*, *Phys. Rev. C* **92** (2015) 034906 [arXiv:1306.0121].

[19] I.P. Lokhtin and A.M. Snigirev, *A Model of jet quenching in ultrarelativistic heavy ion collisions and high-*p_T *hadron spectra at RHIC*, *Eur. Phys. J. C* **45** (2006) 211 [hep-ph/0506189].

[20] CMS Tracker Group collaboration, *The CMS Phase-1 pixel detector upgrade*, 2021 *JINST* **16** P02027 [arXiv:2012.14304].

[21] CMS collaboration, *Strategies and performance of the CMS silicon tracker alignment during LHC Run 2*, *Nucl. Instrum. Meth. A* **1037** (2022) 166795 [arXiv:2111.08757].

[22] CMS collaboration, *Observation and studies of jet quenching in PbPb collisions at nucleon-nucleon center-of-mass energy = 2.76 TeV*, *Phys. Rev. C* **84** (2011) 024906 [arXiv:1102.1957].

[23] CMS collaboration, *Precision luminosity measurement in proton-proton collisions at* $\sqrt{s}$ = 13 *TeV in 2015 and 2016 at CMS*, *Eur. Phys. J. C* **81** (2021) 800 [arXiv:2104.01927].

[24] CMS collaboration, *CMS luminosity measurement using 2016 proton-nucleus collisions at nucleon-nucleon center-of-mass energy of 8.16 TeV*, CMS-PAS-LUM-17-002, CERN, Geneva (2018).

[25] CMS collaboration, *Luminosity measurement in proton-proton collisions at 5.02 TeV in 2017 at CMS*, CMS-PAS-LUM-19-001, CERN, Geneva (2021).

[26] CMS collaboration, *CMS luminosity measurement using nucleus-nucleus collisions at* $\sqrt{s_{\rm NN}}$ = 5.02 *TeV in 2018*, CMS-PAS-LUM-18-001, CERN, Geneva (2022).

[27] CMS collaboration, *Performance of the CMS muon trigger system in proton-proton collisions at* $\sqrt{s}$ = 13 *TeV*, 2021 *JINST* **16** P07001 [arXiv:2102.04790].

[28] CMS collaboration, *Description and performance of track and primary-vertex reconstruction with the CMS tracker*, 2014 *JINST* **9** P10009 [arXiv:1405.6569].

[29] CMS collaboration, *Performance of the CMS muon detector and muon reconstruction with proton-proton collisions at* $\sqrt{s}$ = 13 *TeV*, 2018 *JINST* **13** P06015 [arXiv:1804.04528].

[30] CMS collaboration, *Performance of CMS muon reconstruction in cosmic-ray events*, 2010 *JINST* **5** T03022 [arXiv:0911.4994].

[31] CMS collaboration, *Particle-flow reconstruction and global event description with the CMS detector*, 2017 *JINST* **12** P10003 [arXiv:1706.04965].

[32] CMS collaboration, *Constraints on the Initial State of Pb-Pb Collisions via Measurements of Z-Boson Yields and Azimuthal Anisotropy at* $\sqrt{s_{NN}}$ = 5.02 *TeV*, *Phys. Rev. Lett.* **127** (2021) 102002 [arXiv:2103.14089].

[33] CMS collaboration, *Using Z Boson Events to Study Parton-Medium Interactions in Pb-Pb Collisions*, *Phys. Rev. Lett.* **128** (2022) 122301 [arXiv:2103.04377].

[34] CMS collaboration, *Study of W boson production in PbPb and* pp *collisions at* $\sqrt{s_{NN}}$ = 2.76 *TeV*, *Phys. Lett. B* **715** (2012) 66 [arXiv:1205.6334].

[35] CMS collaboration, *Evidence for Top Quark Production in Nucleus-Nucleus Collisions*, *Phys. Rev. Lett.* **125** (2020) 222001 [arXiv:2006.11110].

[36] CMS collaboration, *CMS Physics: Technical Design Report Volume 1: Detector Performance and Software*, CERN-LHCC-2006-001, CERN, Geneva (2006).

[37] CMS collaboration, *Description and performance of track and primary-vertex reconstruction with the CMS tracker*, 2014 *JINST* **9** P10009 [arXiv:1405.6569].

[38] Particle Data Group collaboration, *Review of Particle Physics*, *PTEP* **2020** (2020) 083C01.

[39] M. Oreglia, *A Study of the Reactions* $\psi' \to \gamma\gamma\psi$, Ph.D. thesis, Stanford University, Stanford, U.S.A. (1980), SLAC Report SLAC-R-236, Appendix D.

[40] Y. Sun, V. Greco and X.-N. Wang, *Modification of Z^0 leptonic invariant mass in ultrarelativistic heavy ion collisions as a measure of the electromagnetic field*, *Phys. Lett. B* **827** (2022) 136962 [arXiv:2111.01716].

[41] CMS collaboration, *Measurement of Momentum Scale and Resolution of the CMS Detector using Low-mass Resonances and Cosmic Ray Muons*, CMS-PAS-TRK-10-004, CERN, Geneva (2010).

[42] CMS collaboration, *Indications of suppression of excited Υ states in PbPb collisions at $\sqrt{S_{NN}} = 2.76$ TeV*, *Phys. Rev. Lett.* **107** (2011) 052302 [arXiv:1105.4894].

[43] CMS collaboration, *Observation of Sequential Υ Suppression in PbPb Collisions*, *Phys. Rev. Lett.* **109** (2012) 222301 [*Erratum ibid.* **120** (2018) 199903] [arXiv:1208.2826].

[44] CMS collaboration, *Measurement of Prompt $\psi(2S) \to J/\psi$ Yield Ratios in Pb-Pb and $p-p$ Collisions at $\sqrt{s_{NN}} = 2.76$ TeV*, *Phys. Rev. Lett.* **113** (2014) 262301 [arXiv:1410.1804].

[45] CMS collaboration, *Relative Modification of Prompt $\psi(2S)$ and J/ψ Yields from pp to PbPb Collisions at $\sqrt{s_{NN}} = 5.02$ TeV*, *Phys. Rev. Lett.* **118** (2017) 162301 [arXiv:1611.01438].

[46] CMS collaboration, *Suppression of $\Upsilon(1S)$, $\Upsilon(2S)$ and $\Upsilon(3S)$ production in PbPb collisions at $\sqrt{s_{\rm NN}} = 2.76$ TeV*, *Phys. Lett. B* **770** (2017) 357 [arXiv:1611.01510].

[47] CMS collaboration, *Suppression and azimuthal anisotropy of prompt and nonprompt J/ψ production in PbPb collisions at $\sqrt{s_{_{\mathrm{NN}}}} = 2.76$* TeV, *Eur. Phys. J. C* **77** (2017) 252 [arXiv:1610.00613].

[48] CMS collaboration, *Suppression of Excited Υ States Relative to the Ground State in Pb-Pb Collisions at $\sqrt{s_{\rm NN}} = 5.02$ TeV*, *Phys. Rev. Lett.* **120** (2018) 142301 [arXiv:1706.05984].

[49] CMS collaboration, *Measurement of prompt and nonprompt charmonium suppression in PbPb collisions at 5.02 TeV* , *Eur. Phys. J. C* **78** (2018) 509 [*Erratum ibid.* **83** (2023) 145] [arXiv:1712.08959].

[50] CMS collaboration, *Measurement of nuclear modification factors of Υ(1S), Υ(2S), and Υ(3S) mesons in PbPb collisions at $\sqrt{s_{_{\mathrm{NN}}}} = 5.02$ TeV*, *Phys. Lett. B* **790** (2019) 270 [arXiv:1805.09215].

[51] CMS collaboration, *Measurement of the azimuthal anisotropy of $\Upsilon(1S)$ and $\Upsilon(2S)$ mesons in PbPb collisions at $\sqrt{s_{NN}} = 5.02$ TeV*, *Phys. Lett. B* **819** (2021) 136385 [arXiv:2006.07707].

[52] CMS collaboration, *Observation of the B_c^+ Meson in Pb-Pb and pp Collisions at $\sqrt{s_{NN}} = 5.02$ TeV and Measurement of its Nuclear Modification Factor*, *Phys. Rev. Lett.* **128** (2022) 252301 [arXiv:2201.02659].

[53] CMS collaboration, *Study of Jet Quenching with Z + jet Correlations in Pb-Pb and pp Collisions at $\sqrt{s}_{NN} = 5.02$* TeV, *Phys. Rev. Lett.* **119** (2017) 082301 [arXiv:1702.01060].

[54] CMS collaboration, *Study of Z boson production in PbPb collisions at $\sqrt{s_{NN}} = 2.76$ TeV*, *Phys. Rev. Lett.* **106** (2011) 212301 [arXiv:1102.5435].

2024 JINST 19 P09012

The CMS collaboration

Yerevan Physics Institute, Yerevan, Armenia

A. Hayrapetyan, A. Tumasyan[1]

Institut für Hochenergiephysik, Vienna, Austria

W. Adam, J.W. Andrejkovic, T. Bergauer, S. Chatterjee, K. Damanakis, M. Dragicevic, P.S. Hussain, M. Jeitler[2], N. Krammer, A. Li, D. Liko, I. Mikulec, J. Schieck[2], R. Schöfbeck, D. Schwarz, M. Sonawane, S. Templ, W. Waltenberger, C.-E. Wulz[2]

Universiteit Antwerpen, Antwerpen, Belgium

M.R. Darwish[3], T. Janssen, P. Van Mechelen

Vrije Universiteit Brussel, Brussel, Belgium

E.S. Bols, J. D'Hondt, S. Dansana, A. De Moor, M. Delcourt, H. El Faham, S. Lowette, I. Makarenko, D. Müller, A.R. Sahasransu, S. Tavernier, M. Tytgat[4], S. Van Putte, D. Vannerom

Université Libre de Bruxelles, Bruxelles, Belgium

B. Clerbaux, G. De Lentdecker, L. Favart, D. Hohov, J. Jaramillo, A. Khalilzadeh, K. Lee, M. Mahdavikhorrami, A. Malara, S. Paredes, L. Pétré, N. Postiau, L. Thomas, M. Vanden Bemden, C. Vander Velde, P. Vanlaer

Ghent University, Ghent, Belgium

M. De Coen, D. Dobur, Y. Hong, J. Knolle, L. Lambrecht, G. Mestdach, C. Rendón, A. Samalan, K. Skovpen, N. Van Den Bossche, J. van der Linden, L. Wezenbeek

Université Catholique de Louvain, Louvain-la-Neuve, Belgium

A. Benecke, G. Bruno, C. Caputo, C. Delaere, I.S. Donertas, A. Giammanco, K. Jaffel, Sa. Jain, V. Lemaitre, J. Lidrych, P. Mastrapasqua, K. Mondal, T.T. Tran, S. Wertz

Centro Brasileiro de Pesquisas Fisicas, Rio de Janeiro, Brazil

G.A. Alves, E. Coelho, C. Hensel, T. Menezes De Oliveira, A. Moraes, P. Rebello Teles, M. Soeiro

Universidade do Estado do Rio de Janeiro, Rio de Janeiro, Brazil

W.L. Aldá Júnior, M. Alves Gallo Pereira, M. Barroso Ferreira Filho, H. Brandao Malbouisson, W. Carvalho, J. Chinellato[5], E.M. Da Costa, G.G. Da Silveira[6], D. De Jesus Damiao, S. Fonseca De Souza, R. Gomes De Souza, J. Martins[7], C. Mora Herrera, K. Mota Amarilo, L. Mundim, H. Nogima, A. Santoro, A. Sznajder, M. Thiel, A. Vilela Pereira

Universidade Estadual Paulista, Universidade Federal do ABC, São Paulo, Brazil

C.A. Bernardes[6], L. Calligaris, T.R. Fernandez Perez Tomei, E.M. Gregores, P.G. Mercadante, S.F. Novaes, B. Orzari, Sandra S. Padula

Institute for Nuclear Research and Nuclear Energy, Bulgarian Academy of Sciences, Sofia, Bulgaria
A. Aleksandrov, G. Antchev, R. Hadjiiska, P. Iaydjiev, M. Misheva, M. Shopova, G. Sultanov

University of Sofia, Sofia, Bulgaria
A. Dimitrov, L. Litov, B. Pavlov, P. Petkov, A. Petrov, E. Shumka

Instituto De Alta Investigación, Universidad de Tarapacá, Casilla 7 D, Arica, Chile
S. Keshri, S. Thakur

Beihang University, Beijing, China
T. Cheng, Q. Guo, T. Javaid, L. Yuan

Department of Physics, Tsinghua University, Beijing, China
Z. Hu, J. Liu, K. Yi[8,9]

Institute of High Energy Physics, Beijing, China
E. Chapon, G.M. Chen[10], H.S. Chen[10], M. Chen[10], F. Iemmi, C.H. Jiang, A. Kapoor[11], H. Liao, Z.-A. Liu[12], R. Sharma[13], J.N. Song[12], J. Tao, C. Wang[10], J. Wang, Z. Wang[10], H. Zhang

State Key Laboratory of Nuclear Physics and Technology, Peking University, Beijing, China
A. Agapitos, Y. Ban, A. Levin, C. Li, Q. Li, Y. Mao, S.J. Qian, X. Sun, D. Wang, H. Yang, L. Zhang, C. Zhou

Sun Yat-Sen University, Guangzhou, China
Z. You

University of Science and Technology of China, Hefei, China
N. Lu

Nanjing Normal University, Nanjing, China
G. Bauer[14]

Institute of Modern Physics and Key Laboratory of Nuclear Physics and Ion-beam Application (MOE) - Fudan University, Shanghai, China
X. Gao[15], D. Leggat, H. Okawa, Y. Zhang

Zhejiang University, Hangzhou, Zhejiang, China
Z. Lin, C. Lu, M. Xiao

Universidad de Los Andes, Bogota, Colombia
C. Avila, D.A. Barbosa Trujillo, A. Cabrera, C. Florez, J. Fraga, J.A. Reyes Vega

Universidad de Antioquia, Medellin, Colombia
J. Mejia Guisao, F. Ramirez, M. Rodriguez, J.D. Ruiz Alvarez

2024 JINST 19 P09012

University of Split, Faculty of Electrical Engineering, Mechanical Engineering and Naval Architecture, Split, Croatia
D. Giljanovic, N. Godinovic, D. Lelas, A. Sculac

University of Split, Faculty of Science, Split, Croatia
M. Kovac, T. Sculac

Institute Rudjer Boskovic, Zagreb, Croatia
P. Bargassa, V. Brigljevic, B.K. Chitroda, D. Ferencek, S. Mishra, A. Starodumov[16], T. Susa

University of Cyprus, Nicosia, Cyprus
A. Attikis, K. Christoforou, S. Konstantinou, J. Mousa, C. Nicolaou, F. Ptochos, P.A. Razis, H. Rykaczewski, H. Saka, A. Stepennov

Charles University, Prague, Czech Republic
M. Finger, M. Finger Jr., A. Kveton

Escuela Politecnica Nacional, Quito, Ecuador
E. Ayala

Universidad San Francisco de Quito, Quito, Ecuador
E. Carrera Jarrin

Academy of Scientific Research and Technology of the Arab Republic of Egypt, Egyptian Network of High Energy Physics, Cairo, Egypt
S. Elgammal[17], A. Ellithi Kamel[18]

Center for High Energy Physics (CHEP-FU), Fayoum University, El-Fayoum, Egypt
M. Abdullah Al-Mashad, M.A. Mahmoud

National Institute of Chemical Physics and Biophysics, Tallinn, Estonia
R.K. Dewanjee[19], K. Ehataht, M. Kadastik, T. Lange, S. Nandan, C. Nielsen, J. Pata, M. Raidal, L. Tani, C. Veelken

Department of Physics, University of Helsinki, Helsinki, Finland
H. Kirschenmann, K. Osterberg, M. Voutilainen

Helsinki Institute of Physics, Helsinki, Finland
S. Bharthuar, E. Brücken, F. Garcia, J. Havukainen, K.T.S. Kallonen, R. Kinnunen, T. Lampén, K. Lassila-Perini, S. Lehti, T. Lindén, M. Lotti, L. Martikainen, M. Myllymäki, M.m. Rantanen, H. Siikonen, E. Tuominen, J. Tuominiemi

Lappeenranta-Lahti University of Technology, Lappeenranta, Finland
P. Luukka, H. Petrow, T. Tuuva[†]

2024 JINST 19 P09012

IRFU, CEA, Université Paris-Saclay, Gif-sur-Yvette, France

M. Besancon, F. Couderc, M. Dejardin, D. Denegri, J.L. Faure, F. Ferri, S. Ganjour, P. Gras, G. Hamel de Monchenault, V. Lohezic, J. Malcles, J. Rander, A. Rosowsky, M.Ö. Sahin, A. Savoy-Navarro[20], P. Simkina, M. Titov, M. Tornago

Laboratoire Leprince-Ringuet, CNRS/IN2P3, Ecole Polytechnique, Institut Polytechnique de Paris, Palaiseau, France

C. Baldenegro Barrera, F. Beaudette, A. Buchot Perraguin, P. Busson, A. Cappati, C. Charlot, F. Damas, O. Davignon, A. De Wit, G. Falmagne, B.A. Fontana Santos Alves, S. Ghosh, A. Gilbert, R. Granier de Cassagnac, A. Hakimi, B. Harikrishnan, L. Kalipoliti, G. Liu, J. Motta, M. Nguyen, C. Ochando, L. Portales, R. Salerno, J.B. Sauvan, Y. Sirois, A. Tarabini, E. Vernazza, A. Zabi, A. Zghiche

Université de Strasbourg, CNRS, IPHC UMR 7178, Strasbourg, France

J.-L. Agram[21], J. Andrea, D. Apparu, D. Bloch, J.-M. Brom, E.C. Chabert, C. Collard, S. Falke, U. Goerlach, C. Grimault, R. Haeberle, A.-C. Le Bihan, M. Meena, G. Saha, M.A. Sessini, P. Van Hove

Institut de Physique des 2 Infinis de Lyon (IP2I), Villeurbanne, France

S. Beauceron, B. Blancon, G. Boudoul, N. Chanon, J. Choi, D. Contardo, P. Depasse, C. Dozen[22], H. El Mamouni, J. Fay, S. Gascon, M. Gouzevitch, C. Greenberg, G. Grenier, B. Ille, I.B. Laktineh, M. Lethuillier, L. Mirabito, S. Perries, A. Purohit, M. Vander Donckt, P. Verdier, J. Xiao

Georgian Technical University, Tbilisi, Georgia

I. Bagaturia[23], I. Lomidze, Z. Tsamalaidze[16]

RWTH Aachen University, I. Physikalisches Institut, Aachen, Germany

V. Botta, L. Feld, K. Klein, M. Lipinski, D. Meuser, A. Pauls, N. Röwert, M. Teroerde

RWTH Aachen University, III. Physikalisches Institut A, Aachen, Germany

S. Diekmann, A. Dodonova, N. Eich, D. Eliseev, F. Engelke, J. Erdmann, M. Erdmann, P. Fackeldey, B. Fischer, T. Hebbeker, K. Hoepfner, F. Ivone, A. Jung, M.y. Lee, L. Mastrolorenzo, F. Mausolf, M. Merschmeyer, A. Meyer, S. Mukherjee, D. Noll, A. Novak, F. Nowotny, A. Pozdnyakov, Y. Rath, W. Redjeb, F. Rehm, H. Reithler, U. Sarkar, V. Sarkisovi, A. Schmidt, A. Sharma, J.L. Spah, A. Stein, F. Torres Da Silva De Araujo[24], L. Vigilante, S. Wiedenbeck, S. Zaleski

RWTH Aachen University, III. Physikalisches Institut B, Aachen, Germany

C. Dziwok, G. Flügge, W. Haj Ahmad[25], T. Kress, A. Nowack, O. Pooth, A. Stahl, T. Ziemons, A. Zotz

Deutsches Elektronen-Synchrotron, Hamburg, Germany

H. Aarup Petersen, M. Aldaya Martin, J. Alimena, S. Amoroso, Y. An, S. Baxter, M. Bayatmakou, H. Becerril Gonzalez, O. Behnke, A. Belvedere, S. Bhattacharya, F. Blekman[26], K. Borras[27], D. Brunner, A. Campbell, A. Cardini, C. Cheng, F. Colombina,

2024 JINST 19 P09012

S. Consuegra Rodríguez, G. Correia Silva, M. De Silva, G. Eckerlin, D. Eckstein, L.I. Estevez Banos, O. Filatov, E. Gallo[26], A. Geiser, A. Giraldi, G. Greau, V. Guglielmi, M. Guthoff, A. Hinzmann, A. Jafari[28], L. Jeppe, N.Z. Jomhari, B. Kaech, M. Kasemann, H. Kaveh, C. Kleinwort, R. Kogler, M. Komm, D. Krücker, W. Lange, D. Leyva Pernia, K. Lipka[29], W. Lohmann[30], R. Mankel, I.-A. Melzer-Pellmann, M. Mendizabal Morentin, J. Metwally, A.B. Meyer, G. Milella, A. Mussgiller, L.P. Nair, A. Nürnberg, Y. Otarid, J. Park, D. Pérez Adán, E. Ranken, A. Raspereza, B. Ribeiro Lopes, J. Rübenach, A. Saggio, M. Scham[31,27], S. Schnake[27], P. Schütze, C. Schwanenberger[26], D. Selivanova, M. Shchedrolosiev, R.E. Sosa Ricardo, D. Stafford, F. Vazzoler, A. Ventura Barroso, R. Walsh, Q. Wang, Y. Wen, K. Wichmann, L. Wiens[27], C. Wissing, Y. Yang, A. Zimermmane Castro Santos

University of Hamburg, Hamburg, Germany

A. Albrecht, S. Albrecht, M. Antonello, S. Bein, L. Benato, M. Bonanomi, P. Connor, M. Eich, K. El Morabit, Y. Fischer, A. Fröhlich, C. Garbers, E. Garutti, A. Grohsjean, M. Hajheidari, J. Haller, H.R. Jabusch, G. Kasieczka, P. Keicher, R. Klanner, W. Korcari, T. Kramer, V. Kutzner, F. Labe, J. Lange, A. Lobanov, C. Matthies, A. Mehta, L. Moureaux, M. Mrowietz, A. Nigamova, Y. Nissan, A. Paasch, K.J. Pena Rodriguez, T. Quadfasel, B. Raciti, M. Rieger, D. Savoiu, J. Schindler, P. Schleper, M. Schröder, J. Schwandt, M. Sommerhalder, H. Stadie, G. Steinbrück, A. Tews, M. Wolf

Karlsruher Institut fuer Technologie, Karlsruhe, Germany

S. Brommer, M. Burkart, E. Butz, T. Chwalek, A. Dierlamm, A. Droll, N. Faltermann, M. Giffels, A. Gottmann, F. Hartmann[32], R. Hofsaess, M. Horzela, U. Husemann, J. Kieseler, M. Klute, R. Koppenhöfer, J.M. Lawhorn, M. Link, A. Lintuluoto, S. Maier, S. Mitra, M. Mormile, Th. Müller, M. Neukum, M. Oh, M. Presilla, G. Quast, K. Rabbertz, B. Regnery, N. Shadskiy, I. Shvetsov, H.J. Simonis, M. Toms[33], N. Trevisani, R. Ulrich, R.F. Von Cube, M. Wassmer, S. Wieland, F. Wittig, R. Wolf, S. Wunsch, X. Zuo

Institute of Nuclear and Particle Physics (INPP), NCSR Demokritos, Aghia Paraskevi, Greece

G. Anagnostou, G. Daskalakis, A. Kyriakis, A. Papadopoulos[32], A. Stakia

National and Kapodistrian University of Athens, Athens, Greece

P. Kontaxakis, G. Melachroinos, A. Panagiotou, I. Papavergou, I. Paraskevas, N. Saoulidou, K. Theofilatos, E. Tziaferi, K. Vellidis, I. Zisopoulos

National Technical University of Athens, Athens, Greece

G. Bakas, T. Chatzistavrou, G. Karapostoli, K. Kousouris, I. Papakrivopoulos, E. Siamarkou, G. Tsipolitis, A. Zacharopoulou

University of Ioánnina, Ioánnina, Greece

K. Adamidis, I. Bestintzanos, I. Evangelou, C. Foudas, P. Gianneios, C. Kamtsikis, P. Katsoulis, P. Kokkas, P.G. Kosmoglou Kioseoglou, N. Manthos, I. Papadopoulos, J. Strologas

HUN-REN Wigner Research Centre for Physics, Budapest, Hungary

M. Bartók[34], C. Hajdu, D. Horvath[35,36], F. Sikler, V. Veszpremi

2024 JINST 19 P09012

MTA-ELTE Lendület CMS Particle and Nuclear Physics Group, Eötvös Loránd University, Budapest, Hungary
M. Csanád, K. Farkas, M.M.A. Gadallah[37], Á. Kadlecsik, P. Major, K. Mandal, G. Pásztor, A.J. Rádl[38], G.I. Veres

Faculty of Informatics, University of Debrecen, Debrecen, Hungary
P. Raics, B. Ujvari, G. Zilizi

Institute of Nuclear Research ATOMKI, Debrecen, Hungary
G. Bencze, S. Czellar, J. Karancsi[34], J. Molnar, Z. Szillasi

Karoly Robert Campus, MATE Institute of Technology, Gyongyos, Hungary
T. Csorgo[38], F. Nemes[38], T. Novak

Panjab University, Chandigarh, India
J. Babbar, S. Bansal, S.B. Beri, V. Bhatnagar, G. Chaudhary, S. Chauhan, N. Dhingra[39], A. Kaur, A. Kaur, H. Kaur, M. Kaur, S. Kumar, K. Sandeep, T. Sheokand, J.B. Singh, A. Singla

University of Delhi, Delhi, India
A. Ahmed, A. Bhardwaj, A. Chhetri, B.C. Choudhary, A. Kumar, A. Kumar, M. Naimuddin, K. Ranjan, S. Saumya

Saha Institute of Nuclear Physics, HBNI, Kolkata, India
S. Baradia, S. Barman[40], S. Bhattacharya, S. Dutta, S. Dutta, P. Palit, S. Sarkar

Indian Institute of Technology Madras, Madras, India
M.M. Ameen, P.K. Behera, S.C. Behera, S. Chatterjee, P. Jana, P. Kalbhor, J.R. Komaragiri[41], D. Kumar[41], L. Panwar[41], P.R. Pujahari, N.R. Saha, A. Sharma, A.K. Sikdar, S. Verma

Tata Institute of Fundamental Research-A, Mumbai, India
S. Dugad, M. Kumar, G.B. Mohanty, P. Suryadevara

Tata Institute of Fundamental Research-B, Mumbai, India
A. Bala, S. Banerjee, R.M. Chatterjee, M. Guchait, Sh. Jain, S. Karmakar, S. Kumar, G. Majumder, K. Mazumdar, S. Parolia, A. Thachayath

National Institute of Science Education and Research, An OCC of Homi Bhabha National Institute, Bhubaneswar, Odisha, India
S. Bahinipati[42], A.K. Das, C. Kar, D. Maity[43], P. Mal, T. Mishra, V.K. Muraleedharan Nair Bindhu[43], K. Naskar[43], A. Nayak[43], P. Sadangi, P. Saha, S.K. Swain, S. Varghese[43], D. Vats[43]

Indian Institute of Science Education and Research (IISER), Pune, India
S. Acharya[44], A. Alpana, S. Dube, B. Gomber[44], B. Kansal, A. Laha, B. Sahu[44], S. Sharma

Isfahan University of Technology, Isfahan, Iran
H. Bakhshiansohi[45], E. Khazaie[46], M. Zeinali[47]

Institute for Research in Fundamental Sciences (IPM), Tehran, Iran
S. Chenarani[48], S.M. Etesami, M. Khakzad, M. Mohammadi Najafabadi

University College Dublin, Dublin, Ireland
M. Grunewald

INFN Sezione di Bari[a], Università di Bari[b], Politecnico di Bari[c], Bari, Italy
M. Abbrescia[a,b], R. Aly[a,c,49], A. Colaleo[a,b], D. Creanza[a,c], B. D'Anzi[a,b], N. De Filippis[a,c], M. De Palma[a,b], A. Di Florio[a,c], W. Elmetenawee[a,b,49], L. Fiore[a], G. Iaselli[a,c], M. Louka[a,b], G. Maggi[a,c], M. Maggi[a], I. Margjeka[a,b], V. Mastrapasqua[a,b], S. My[a,b], S. Nuzzo[a,b], A. Pellecchia[a,b], A. Pompili[a,b], G. Pugliese[a,c], R. Radogna[a], G. Ramirez-Sanchez[a,c], D. Ramos[a], A. Ranieri[a], L. Silvestris[a], F.M. Simone[a,b], Ü. Sözbilir[a], A. Stamerra[a], R. Venditti[a], P. Verwilligen[a], A. Zaza[a,b]

INFN Sezione di Bologna[a], Università di Bologna[b], Bologna, Italy
G. Abbiendi[a], C. Battilana[a,b], D. Bonacorsi[a,b], L. Borgonovi[a], P. Capiluppi[a,b], A. Castro[a,b], F.R. Cavallo[a], M. Cuffiani[a,b], G.M. Dallavalle[a], T. Diotalevi[a,b], F. Fabbri[a], A. Fanfani[a,b], D. Fasanella[a,b], P. Giacomelli[a], L. Giommi[a,b], C. Grandi[a], L. Guiducci[a,b], S. Lo Meo[a,50], L. Lunerti[a,b], S. Marcellini[a], G. Masetti[a], F.L. Navarria[a,b], A. Perrotta[a], F. Primavera[a,b], A.M. Rossi[a,b], T. Rovelli[a,b], G.P. Siroli[a,b]

INFN Sezione di Catania[a], Università di Catania[b], Catania, Italy
S. Costa[a,b,51], A. Di Mattia[a], R. Potenza[a,b], A. Tricomi[a,b,51], C. Tuve[a,b]

INFN Sezione di Firenze[a], Università di Firenze[b], Firenze, Italy
P. Assiouras[a], G. Barbagli[a], G. Bardelli[a,b], B. Camaiani[a,b], A. Cassese[a], R. Ceccarelli[a], V. Ciulli[a,b], C. Civinini[a], R. D'Alessandro[a,b], E. Focardi[a,b], T. Kello[a], G. Latino[a,b], P. Lenzi[a,b], M. Lizzo[a], M. Meschini[a], S. Paoletti[a], A. Papanastassiou[a,b], G. Sguazzoni[a], L. Viliani[a]

INFN Laboratori Nazionali di Frascati, Frascati, Italy
L. Benussi, S. Bianco, S. Meola[52], D. Piccolo

INFN Sezione di Genova[a], Università di Genova[b], Genova, Italy
P. Chatagnon[a], F. Ferro[a], E. Robutti[a], S. Tosi[a,b]

INFN Sezione di Milano-Bicocca[a], Università di Milano-Bicocca[b], Milano, Italy
A. Benaglia[a], G. Boldrini[a,b], F. Brivio[a], F. Cetorelli[a], F. De Guio[a,b], M.E. Dinardo[a,b], P. Dini[a], S. Gennai[a], R. Gerosa[a,b], A. Ghezzi[a,b], P. Govoni[a,b], L. Guzzi[a], M.T. Lucchini[a,b], M. Malberti[a], S. Malvezzi[a], A. Massironi[a], D. Menasce[a], L. Moroni[a], M. Paganoni[a,b], D. Pedrini[a], B.S. Pinolini[a], S. Ragazzi[a,b], T. Tabarelli de Fatis[a,b], D. Zuolo[a]

INFN Sezione di Napoli[a], Università di Napoli 'Federico II'[b], Napoli, Italy; Università della Basilicata[c], Potenza, Italy; Scuola Superiore Meridionale (SSM)[d], Napoli, Italy
S. Buontempo[a], A. Cagnotta[a,b], F. Carnevali[a,b], N. Cavallo[a,c], A. De Iorio[a,b], F. Fabozzi[a,c], A.O.M. Iorio[a,b], L. Lista[a,b,53], P. Paolucci[a,32], B. Rossi[a], C. Sciacca[a,b]

2024 JINST 19 P09012

INFN Sezione di Padova[a], Università di Padova[b], Padova, Italy; Università di Trento[c], Trento, Italy

R. Ardino[a], P. Azzi[a], N. Bacchetta[a,54], D. Bisello[a,b], P. Bortignon[a], A. Bragagnolo[a,b], T. Dorigo[a], F. Gasparini[a,b], U. Gasparini[a,b], E. Lusiani[a], M. Margoni[a,b], G. Maron[a,55], A.T. Meneguzzo[a,b], M. Michelotto[a], M. Migliorini[a,b], J. Pazzini[a,b], P. Ronchese[a,b], R. Rossin[a,b], F. Simonetto[a,b], G. Strong[a], M. Tosi[a,b], A. Triossi[a,b], S. Ventura[a], H. Yarar[a,b], M. Zanetti[a,b], P. Zotto[a,b], A. Zucchetta[a,b], G. Zumerle[a,b]

INFN Sezione di Pavia[a], Università di Pavia[b], Pavia, Italy

S. Abu Zeid[a,56], C. Aimè[a,b], A. Braghieri[a], S. Calzaferri[a], D. Fiorina[a], P. Montagna[a,b], V. Re[a], C. Riccardi[a,b], P. Salvini[a], I. Vai[a,b], P. Vitulo[a,b]

INFN Sezione di Perugia[a], Università di Perugia[b], Perugia, Italy

S. Ajmal[a,b], P. Asenov[a,57], G.M. Bilei[a], D. Ciangottini[a,b], L. Fanò[a,b], M. Magherini[a,b], G. Mantovani[a,b], V. Mariani[a,b], M. Menichelli[a], F. Moscatelli[a,57], A. Rossi[a,b], A. Santocchia[a,b], D. Spiga[a], T. Tedeschi[a,b]

INFN Sezione di Pisa[a], Università di Pisa[b], Scuola Normale Superiore di Pisa[c], Pisa, Italy; Università di Siena[d], Siena, Italy

P. Azzurri[a], G. Bagliesi[a], R. Bhattacharya[a], L. Bianchini[a,b], T. Boccali[a], E. Bossini[a], D. Bruschini[a,c], R. Castaldi[a], M.A. Ciocci[a,b], M. Cipriani[a,b], V. D'Amante[a,d], R. Dell'Orso[a], S. Donato[a], A. Giassi[a], F. Ligabue[a,c], D. Matos Figueiredo[a], A. Messineo[a,b], M. Musich[a,b], F. Palla[a], A. Rizzi[a,b], G. Rolandi[a,c], S. Roy Chowdhury[a], T. Sarkar[a], A. Scribano[a], P. Spagnolo[a], R. Tenchini[a], G. Tonelli[a,b], N. Turini[a,d], A. Venturi[a], P.G. Verdini[a]

INFN Sezione di Roma[a], Sapienza Università di Roma[b], Roma, Italy

P. Barria[a], M. Campana[a,b], F. Cavallari[a], L. Cunqueiro Mendez[a,b], D. Del Re[a,b], E. Di Marco[a], M. Diemoz[a], F. Errico[a,b], E. Longo[a,b], P. Meridiani[a], J. Mijuskovic[a,b], G. Organtini[a,b], F. Pandolfi[a], R. Paramatti[a,b], C. Quaranta[a,b], S. Rahatlou[a,b], C. Rovelli[a], F. Santanastasio[a,b], L. Soffi[a]

INFN Sezione di Torino[a], Università di Torino[b], Torino, Italy; Università del Piemonte Orientale[c], Novara, Italy

N. Amapane[a,b], R. Arcidiacono[a,c], S. Argiro[a,b], M. Arneodo[a,c], N. Bartosik[a], R. Bellan[a,b], A. Bellora[a,b], C. Biino[a], N. Cartiglia[a], M. Costa[a,b], R. Covarelli[a,b], N. Demaria[a], L. Finco[a], M. Grippo[a,b], B. Kiani[a,b], F. Legger[a], F. Luongo[a,b], C. Mariotti[a], S. Maselli[a], A. Mecca[a,b], E. Migliore[a,b], M. Monteno[a], R. Mulargia[a], M.M. Obertino[a,b], G. Ortona[a], L. Pacher[a,b], N. Pastrone[a], M. Pelliccioni[a], M. Ruspa[a,c], F. Siviero[a,b], V. Sola[a,b], A. Solano[a,b], A. Staiano[a], C. Tarricone[a,b], D. Trocino[a], G. Umoret[a,b], E. Vlasov[a,b]

INFN Sezione di Trieste[a], Università di Trieste[b], Trieste, Italy

S. Belforte[a], V. Candelise[a,b], M. Casarsa[a], F. Cossutti[a], K. De Leo[a,b], G. Della Ricca[a,b]

Kyungpook National University, Daegu, Korea

S. Dogra, J. Hong, C. Huh, B. Kim, D.H. Kim, J. Kim, H. Lee, S.W. Lee, C.S. Moon, Y.D. Oh, M.S. Ryu, S. Sekmen, Y.C. Yang

2024 JINST 19 P09012

Department of Mathematics and Physics - GWNU, Gangneung, Korea
M.S. Kim

Chonnam National University, Institute for Universe and Elementary Particles, Kwangju, Korea
G. Bak, P. Gwak, H. Kim, D.H. Moon

Hanyang University, Seoul, Korea
E. Asilar, D. Kim, T.J. Kim, J.A. Merlin

Korea University, Seoul, Korea
S. Choi, S. Han, B. Hong, K. Lee, K.S. Lee, S. Lee, J. Park, S.K. Park, J. Yoo

Kyung Hee University, Department of Physics, Seoul, Korea
J. Goh, S. Yang

Sejong University, Seoul, Korea
H. S. Kim, Y. Kim, S. Lee

Seoul National University, Seoul, Korea
J. Almond, J.H. Bhyun, J. Choi, W. Jun, J. Kim, J.S. Kim, S. Ko, H. Kwon, H. Lee, J. Lee, J. Lee, B.H. Oh, S.B. Oh, H. Seo, U.K. Yang, I. Yoon

University of Seoul, Seoul, Korea
W. Jang, D.Y. Kang, Y. Kang, S. Kim, B. Ko, J.S.H. Lee, Y. Lee, I.C. Park, Y. Roh, I.J. Watson

Yonsei University, Department of Physics, Seoul, Korea
S. Ha, H.D. Yoo

Sungkyunkwan University, Suwon, Korea
M. Choi, M.R. Kim, H. Lee, Y. Lee, I. Yu

College of Engineering and Technology, American University of the Middle East (AUM), Dasman, Kuwait
T. Beyrouthy, Y. Maghrbi

Riga Technical University, Riga, Latvia
K. Dreimanis, A. Gaile, G. Pikurs, A. Potrebko, M. Seidel, V. Veckalns[58]

University of Latvia (LU), Riga, Latvia
N.R. Strautnieks

Vilnius University, Vilnius, Lithuania
M. Ambrozas, A. Juodagalvis, A. Rinkevicius, G. Tamulaitis

National Centre for Particle Physics, Universiti Malaya, Kuala Lumpur, Malaysia
N. Bin Norjoharuddeen, I. Yusuff[59], Z. Zolkapli

Universidad de Sonora (UNISON), Hermosillo, Mexico
J.F. Benitez, A. Castaneda Hernandez, H.A. Encinas Acosta, L.G. Gallegos Maríñez, M. León Coello, J.A. Murillo Quijada, A. Sehrawat, L. Valencia Palomo

Centro de Investigacion y de Estudios Avanzados del IPN, Mexico City, Mexico
G. Ayala, H. Castilla-Valdez, E. De La Cruz-Burelo, I. Heredia-De La Cruz[60], R. Lopez-Fernandez, C.A. Mondragon Herrera, A. Sánchez Hernández

Universidad Iberoamericana, Mexico City, Mexico
C. Oropeza Barrera, M. Ramírez García

Benemerita Universidad Autonoma de Puebla, Puebla, Mexico
I. Bautista, I. Pedraza, H.A. Salazar Ibarguen, C. Uribe Estrada

University of Montenegro, Podgorica, Montenegro
I. Bubanja, N. Raicevic

University of Canterbury, Christchurch, New Zealand
P.H. Butler

National Centre for Physics, Quaid-I-Azam University, Islamabad, Pakistan
A. Ahmad, M.I. Asghar, A. Awais, M.I.M. Awan, H.R. Hoorani, W.A. Khan

AGH University of Krakow, Faculty of Computer Science, Electronics and Telecommunications, Krakow, Poland
V. Avati, L. Grzanka, M. Malawski

National Centre for Nuclear Research, Swierk, Poland
H. Bialkowska, M. Bluj, B. Boimska, M. Górski, M. Kazana, M. Szleper, P. Zalewski

Institute of Experimental Physics, Faculty of Physics, University of Warsaw, Warsaw, Poland
K. Bunkowski, K. Doroba, A. Kalinowski, M. Konecki, J. Krolikowski, A. Muhammad

Warsaw University of Technology, Warsaw, Poland
K. Pozniak, W. Zabolotny

Laboratório de Instrumentação e Física Experimental de Partículas, Lisboa, Portugal
M. Araujo, D. Bastos, C. Beirão Da Cruz E Silva, A. Boletti, M. Bozzo, T. Camporesi, G. Da Molin, P. Faccioli, M. Gallinaro, J. Hollar, N. Leonardo, T. Niknejad, A. Petrilli, M. Pisano, J. Seixas, J. Varela, J.W. Wulff

Faculty of Physics, University of Belgrade, Belgrade, Serbia
P. Adzic, P. Milenovic

VINCA Institute of Nuclear Sciences, University of Belgrade, Belgrade, Serbia
M. Dordevic, J. Milosevic, V. Rekovic

2024 JINST 19 P09012

Centro de Investigaciones Energéticas Medioambientales y Tecnológicas (CIEMAT), Madrid, Spain

M. Aguilar-Benitez, J. Alcaraz Maestre, Cristina F. Bedoya, M. Cepeda, M. Cerrada, N. Colino, B. De La Cruz, A. Delgado Peris, A. Escalante Del Valle, D. Fernández Del Val, J.P. Fernández Ramos, J. Flix, M.C. Fouz, O. Gonzalez Lopez, S. Goy Lopez, J.M. Hernandez, M.I. Josa, D. Moran, C. M. Morcillo Perez, Á. Navarro Tobar, C. Perez Dengra, A. Pérez-Calero Yzquierdo, J. Puerta Pelayo, I. Redondo, D.D. Redondo Ferrero, L. Romero, S. Sánchez Navas, L. Urda Gómez, J. Vazquez Escobar, C. Willmott

Universidad Autónoma de Madrid, Madrid, Spain

J.F. de Trocóniz

Universidad de Oviedo, Instituto Universitario de Ciencias y Tecnologías Espaciales de Asturias (ICTEA), Oviedo, Spain

B. Alvarez Gonzalez, J. Cuevas, J. Fernandez Menendez, S. Folgueras, I. Gonzalez Caballero, J.R. González Fernández, E. Palencia Cortezon, C. Ramón Álvarez, V. Rodríguez Bouza, A. Soto Rodríguez, A. Trapote, C. Vico Villalba, P. Vischia

Instituto de Física de Cantabria (IFCA), CSIC-Universidad de Cantabria, Santander, Spain

S. Bhowmik, S. Blanco Fernández, J.A. Brochero Cifuentes, I.J. Cabrillo, A. Calderon, J. Duarte Campderros, M. Fernandez, G. Gomez, C. Lasaosa García, C. Martinez Rivero, P. Martinez Ruiz del Arbol, F. Matorras, P. Matorras Cuevas, E. Navarrete Ramos, J. Piedra Gomez, L. Scodellaro, I. Vila, J.M. Vizan Garcia

University of Colombo, Colombo, Sri Lanka

M.K. Jayananda, B. Kailasapathy[61], D.U.J. Sonnadara, D.D.C. Wickramarathna

University of Ruhuna, Department of Physics, Matara, Sri Lanka

W.G.D. Dharmaratna[62], K. Liyanage, N. Perera, N. Wickramage

CERN, European Organization for Nuclear Research, Geneva, Switzerland

D. Abbaneo, C. Amendola, E. Auffray, G. Auzinger, J. Baechler, D. Barney, A. Bermúdez Martínez, M. Bianco, B. Bilin, A.A. Bin Anuar, A. Bocci, E. Brondolin, C. Caillol, G. Cerminara, N. Chernyavskaya, D. d'Enterria, A. Dabrowski, A. David, A. De Roeck, M.M. Defranchis, M. Deile, M. Dobson, F. Fallavollita[63], L. Forthomme, G. Franzoni, W. Funk, S. Giani, D. Gigi, K. Gill, F. Glege, L. Gouskos, M. Haranko, J. Hegeman, B. Huber, V. Innocente, T. James, P. Janot, S. Laurila, P. Lecoq, E. Leutgeb, C. Lourenço, B. Maier, L. Malgeri, M. Mannelli, A.C. Marini, M. Matthewman, F. Meijers, S. Mersi, E. Meschi, V. Milosevic, F. Monti, F. Moortgat, M. Mulders, I. Neutelings, S. Orfanelli, F. Pantaleo, G. Petrucciani, A. Pfeiffer, M. Pierini, D. Piparo, H. Qu, D. Rabady, G. Reales Gutiérrez, M. Rovere, H. Sakulin, S. Scarfi, C. Schwick, M. Selvaggi, A. Sharma, K. Shchelina, P. Silva, P. Sphicas[64], A.G. Stahl Leiton, A. Steen, S. Summers, D. Treille, P. Tropea, A. Tsirou, D. Walter, J. Wanczyk[65], J. Wang, S. Wuchterl, P. Zehetner, P. Zejdl, W.D. Zeuner

2024 JINST 19 P09012

Paul Scherrer Institut, Villigen, Switzerland

T. Bevilacqua[66], L. Caminada[66], A. Ebrahimi, W. Erdmann, R. Horisberger, Q. Ingram, H.C. Kaestli, D. Kotlinski, C. Lange, M. Missiroli[66], L. Noehte[66], T. Rohe

ETH Zurich - Institute for Particle Physics and Astrophysics (IPA), Zurich, Switzerland

T.K. Aarrestad, K. Androsov[65], M. Backhaus, A. Calandri, C. Cazzaniga, K. Datta, A. De Cosa, G. Dissertori, M. Dittmar, M. Donegà, F. Eble, M. Galli, K. Gedia, F. Glessgen, C. Grab, D. Hits, W. Lustermann, A.-M. Lyon, R.A. Manzoni, M. Marchegiani, L. Marchese, C. Martin Perez, A. Mascellani[65], F. Nessi-Tedaldi, F. Pauss, V. Perovic, S. Pigazzini, M. Reichmann, C. Reissel, T. Reitenspiess, B. Ristic, F. Riti, D. Ruini, D.A. Sanz Becerra, R. Seidita, J. Steggemann[65], D. Valsecchi, R. Wallny

Universität Zürich, Zurich, Switzerland

C. Amsler[67], P. Bärtschi, C. Botta, D. Brzhechko, M.F. Canelli, K. Cormier, R. Del Burgo, J.K. Heikkilä, M. Huwiler, W. Jin, A. Jofrehei, B. Kilminster, S. Leontsinis, S.P. Liechti, A. Macchiolo, P. Meiring, V.M. Mikuni, U. Molinatti, A. Reimers, P. Robmann, S. Sanchez Cruz, K. Schweiger, M. Senger, Y. Takahashi, R. Tramontano

National Central University, Chung-Li, Taiwan

C. Adloff[68], D. Bhowmik, C.M. Kuo, W. Lin, P.K. Rout, P.C. Tiwari[41], S.S. Yu

National Taiwan University (NTU), Taipei, Taiwan

L. Ceard, Y. Chao, K.F. Chen, P.s. Chen, Z.g. Chen, W.-S. Hou, T.h. Hsu, Y.w. Kao, R. Khurana, G. Kole, Y.y. Li, R.-S. Lu, E. Paganis, X.f. Su, J. Thomas-Wilsker, L.s. Tsai, H.y. Wu, E. Yazgan

High Energy Physics Research Unit, Department of Physics, Faculty of Science, Chulalongkorn University, Bangkok, Thailand

C. Asawatangtrakuldee, N. Srimanobhas, V. Wachirapusitanand

Çukurova University, Physics Department, Science and Art Faculty, Adana, Turkey

D. Agyel, F. Boran, Z.S. Demiroglu, F. Dolek, I. Dumanoglu[69], E. Eskut, Y. Guler[70], E. Gurpinar Guler[70], C. Isik, O. Kara, A. Kayis Topaksu, U. Kiminsu, G. Onengut, K. Ozdemir[71], A. Polatoz, B. Tali[72], U.G. Tok, S. Turkcapar, E. Uslan, I.S. Zorbakir

Middle East Technical University, Physics Department, Ankara, Turkey

M. Yalvac[73]

Bogazici University, Istanbul, Turkey

B. Akgun, I.O. Atakisi, E. Gülmez, M. Kaya[74], O. Kaya[75], S. Tekten[76]

Istanbul Technical University, Istanbul, Turkey

A. Cakir, K. Cankocak[69,77], Y. Komurcu, S. Sen[78]

Istanbul University, Istanbul, Turkey

O. Aydilek, S. Cerci[72], V. Epshteyn, B. Hacisahinoglu, I. Hos[79], B. Kaynak, S. Ozkorucuklu, O. Potok, H. Sert, C. Simsek, D. Sunar Cerci[72], C. Zorbilmez

2024 JINST 19 P09012

Yildiz Technical University, Istanbul, Turkey
B. Isildak[80]

Institute for Scintillation Materials of National Academy of Science of Ukraine, Kharkiv, Ukraine
A. Boyaryntsev, B. Grynyov

National Science Centre, Kharkiv Institute of Physics and Technology, Kharkiv, Ukraine
L. Levchuk

University of Bristol, Bristol, United Kingdom
D. Anthony, J.J. Brooke, A. Bundock, F. Bury, E. Clement, D. Cussans, H. Flacher, M. Glowacki, J. Goldstein, H.F. Heath, L. Kreczko, S. Paramesvaran, S. Seif El Nasr-Storey, V.J. Smith, N. Stylianou[81], K. Walkingshaw Pass, R. White

Rutherford Appleton Laboratory, Didcot, United Kingdom
A.H. Ball, K.W. Bell, A. Belyaev[82], C. Brew, R.M. Brown, D.J.A. Cockerill, C. Cooke, K.V. Ellis, K. Harder, S. Harper, M.-L. Holmberg[83], J. Linacre, K. Manolopoulos, D.M. Newbold, E. Olaiya, D. Petyt, T. Reis, G. Salvi, T. Schuh, C.H. Shepherd-Themistocleous, I.R. Tomalin, T. Williams

Imperial College, London, United Kingdom
R. Bainbridge, P. Bloch, C.E. Brown, O. Buchmuller, V. Cacchio, C.A. Carrillo Montoya, G.S. Chahal[84], D. Colling, J.S. Dancu, I. Das, P. Dauncey, G. Davies, J. Davies, M. Della Negra, S. Fayer, G. Fedi, G. Hall, M.H. Hassanshahi, A. Howard, G. Iles, M. Knight, J. Langford, J. León Holgado, L. Lyons, A.-M. Magnan, S. Malik, A. Martelli, M. Mieskolainen, J. Nash[85], M. Pesaresi, B.C. Radburn-Smith, A. Richards, A. Rose, C. Seez, R. Shukla, A. Tapper, K. Uchida, G.P. Uttley, L.H. Vage, T. Virdee[32], M. Vojinovic, N. Wardle, D. Winterbottom

Brunel University, Uxbridge, United Kingdom
K. Coldham, J.E. Cole, A. Khan, P. Kyberd, I.D. Reid

Baylor University, Waco, Texas, USA
S. Abdullin, A. Brinkerhoff, B. Caraway, J. Dittmann, K. Hatakeyama, J. Hiltbrand, B. McMaster, M. Saunders, S. Sawant, C. Sutantawibul, J. Wilson

Catholic University of America, Washington, DC, USA
R. Bartek, A. Dominguez, C. Huerta Escamilla, A.E. Simsek, R. Uniyal, A.M. Vargas Hernandez

The University of Alabama, Tuscaloosa, Alabama, USA
B. Bam, R. Chudasama, S.I. Cooper, S.V. Gleyzer, C.U. Perez, P. Rumerio[86], E. Usai, R. Yi

Boston University, Boston, Massachusetts, USA
A. Akpinar, A. Albert, D. Arcaro, C. Cosby, Z. Demiragli, C. Erice, C. Fangmeier, C. Fernandez Madrazo, E. Fontanesi, D. Gastler, F. Golf, S. Jeon, I. Reed, J. Rohlf, K. Salyer, D. Sperka, D. Spitzbart, I. Suarez, A. Tsatsos, S. Yuan, A.G. Zecchinelli

2024 JINST 19 P09012

Brown University, Providence, Rhode Island, USA
G. Benelli, X. Coubez[27], D. Cutts, M. Hadley, U. Heintz, J.M. Hogan[87], T. Kwon, G. Landsberg, K.T. Lau, D. Li, J. Luo, S. Mondal, M. Narain[†], N. Pervan, S. Sagir[88], F. Simpson, M. Stamenkovic, W.Y. Wong, X. Yan, W. Zhang

University of California, Davis, Davis, California, USA
S. Abbott, J. Bonilla, C. Brainerd, R. Breedon, M. Calderon De La Barca Sanchez, M. Chertok, M. Citron, J. Conway, P.T. Cox, R. Erbacher, H. Folsom, J. Jay, F. Jensen, O. Kukral, G. Mocellin, M. Mulhearn, D. Pellett, W. Wei, Y. Yao, F. Zhang

University of California, Los Angeles, California, USA
M. Bachtis, R. Cousins, A. Datta, G. Flores Avila, J. Hauser, M. Ignatenko, M.A. Iqbal, T. Lam, E. Manca, A. Nunez Del Prado, D. Saltzberg, V. Valuev

University of California, Riverside, Riverside, California, USA
R. Clare, J.W. Gary, M. Gordon, G. Hanson, W. Si, S. Wimpenny[†]

University of California, San Diego, La Jolla, California, USA
J.G. Branson, S. Cittolin, S. Cooperstein, D. Diaz, J. Duarte, L. Giannini, J. Guiang, R. Kansal, V. Krutelyov, R. Lee, J. Letts, M. Masciovecchio, F. Mokhtar, S. Mukherjee, M. Pieri, M. Quinnan, B.V. Sathia Narayanan, V. Sharma, M. Tadel, E. Vourliotis, F. Würthwein, Y. Xiang, A. Yagil

University of California, Santa Barbara - Department of Physics, Santa Barbara, California, USA
A. Barzdukas, L. Brennan, C. Campagnari, A. Dorsett, J. Incandela, J. Kim, A.J. Li, P. Masterson, H. Mei, J. Richman, U. Sarica, R. Schmitz, F. Setti, J. Sheplock, D. Stuart, T.Á. Vámi, S. Wang

California Institute of Technology, Pasadena, California, USA
A. Bornheim, O. Cerri, A. Latorre, J. Mao, H.B. Newman, M. Spiropulu, J.R. Vlimant, C. Wang, S. Xie, R.Y. Zhu

Carnegie Mellon University, Pittsburgh, Pennsylvania, USA
J. Alison, S. An, M.B. Andrews, P. Bryant, M. Cremonesi, V. Dutta, T. Ferguson, A. Harilal, C. Liu, T. Mudholkar, S. Murthy, M. Paulini, A. Roberts, A. Sanchez, W. Terrill

University of Colorado Boulder, Boulder, Colorado, USA
J.P. Cumalat, W.T. Ford, A. Hassani, G. Karathanasis, E. MacDonald, N. Manganelli, F. Marini, A. Perloff, C. Savard, N. Schonbeck, K. Stenson, K.A. Ulmer, S.R. Wagner, N. Zipper

Cornell University, Ithaca, New York, USA
J. Alexander, S. Bright-Thonney, X. Chen, D.J. Cranshaw, J. Fan, X. Fan, D. Gadkari, S. Hogan, P. Kotamnives, J. Monroy, M. Oshiro, J.R. Patterson, J. Reichert, M. Reid, A. Ryd, J. Thom, P. Wittich, R. Zou

2024 JINST 19 P09012

Fermi National Accelerator Laboratory, Batavia, Illinois, USA

M. Albrow, M. Alyari, O. Amram, G. Apollinari, A. Apresyan, L.A.T. Bauerdick, D. Berry, J. Berryhill, P.C. Bhat, K. Burkett, J.N. Butler, A. Canepa, G.B. Cerati, H.W.K. Cheung, F. Chlebana, G. Cummings, J. Dickinson, I. Dutta, V.D. Elvira, Y. Feng, J. Freeman, A. Gandrakota, Z. Gecse, L. Gray, D. Green, A. Grummer, S. Grünendahl, D. Guerrero, O. Gutsche, R.M. Harris, R. Heller, T.C. Herwig, J. Hirschauer, L. Horyn, B. Jayatilaka, S. Jindariani, M. Johnson, U. Joshi, T. Klijnsma, B. Klima, K.H.M. Kwok, S. Lammel, D. Lincoln, R. Lipton, T. Liu, C. Madrid, K. Maeshima, C. Mantilla, D. Mason, P. McBride, P. Merkel, S. Mrenna, S. Nahn, J. Ngadiuba, D. Noonan, V. Papadimitriou, N. Pastika, K. Pedro, C. Pena[89], F. Ravera, A. Reinsvold Hall[90], L. Ristori, E. Sexton-Kennedy, N. Smith, A. Soha, L. Spiegel, S. Stoynev, J. Strait, L. Taylor, S. Tkaczyk, N.V. Tran, L. Uplegger, E.W. Vaandering, I. Zoi

University of Florida, Gainesville, Florida, USA

C. Aruta, P. Avery, D. Bourilkov, L. Cadamuro, P. Chang, V. Cherepanov, R.D. Field, E. Koenig, M. Kolosova, J. Konigsberg, A. Korytov, K.H. Lo, K. Matchev, N. Menendez, G. Mitselmakher, K. Mohrman, A. Muthirakalayil Madhu, N. Rawal, D. Rosenzweig, S. Rosenzweig, K. Shi, J. Wang

Florida State University, Tallahassee, Florida, USA

T. Adams, A. Al Kadhim, A. Askew, N. Bower, R. Habibullah, V. Hagopian, R. Hashmi, R.S. Kim, S. Kim, T. Kolberg, G. Martinez, H. Prosper, P.R. Prova, O. Viazlo, M. Wulansatiti, R. Yohay, J. Zhang

Florida Institute of Technology, Melbourne, Florida, USA

B. Alsufyani, M.M. Baarmand, S. Butalla, T. Elkafrawy[56], M. Hohlmann, R. Kumar Verma, M. Rahmani, E. Yanes

University of Illinois Chicago, Chicago, USA, Chicago, USA

M.R. Adams, A. Baty, C. Bennett, R. Cavanaugh, S. Dittmer, R. Escobar Franco, O. Evdokimov, C.E. Gerber, D.J. Hofman, J.h. Lee, D. S. Lemos, A.H. Merrit, C. Mills, S. Nanda, G. Oh, B. Ozek, D. Pilipovic, R. Pradhan, T. Roy, S. Rudrabhatla, M.B. Tonjes, N. Varelas, X. Wang, Z. Ye, J. Yoo

The University of Iowa, Iowa City, Iowa, USA

M. Alhusseini, D. Blend, K. Dilsiz[91], L. Emediato, G. Karaman, O.K. Köseyan, J.-P. Merlo, A. Mestvirishvili[92], J. Nachtman, O. Neogi, H. Ogul[93], Y. Onel, A. Penzo, C. Snyder, E. Tiras[94]

Johns Hopkins University, Baltimore, Maryland, USA

B. Blumenfeld, L. Corcodilos, J. Davis, A.V. Gritsan, L. Kang, S. Kyriacou, P. Maksimovic, M. Roguljic, J. Roskes, S. Sekhar, M. Swartz

The University of Kansas, Lawrence, Kansas, USA

A. Abreu, L.F. Alcerro Alcerro, J. Anguiano, P. Baringer, A. Bean, Z. Flowers, D. Grove, J. King, G. Krintiras, M. Lazarovits, C. Le Mahieu, C. Lindsey, J. Marquez, N. Minafra,

M. Murray, M. Nickel, M. Pitt, S. Popescu[95], C. Rogan, C. Royon, R. Salvatico, S. Sanders, C. Smith, Q. Wang, G. Wilson

Kansas State University, Manhattan, Kansas, USA

B. Allmond, A. Ivanov, K. Kaadze, A. Kalogeropoulos, D. Kim, Y. Maravin, K. Nam, J. Natoli, D. Roy, G. Sorrentino

Lawrence Livermore National Laboratory, Livermore, California, USA

F. Rebassoo, D. Wright

University of Maryland, College Park, Maryland, USA

A. Baden, A. Belloni, A. Bethani, Y.M. Chen, S.C. Eno, N.J. Hadley, S. Jabeen, R.G. Kellogg, T. Koeth, Y. Lai, S. Lascio, A.C. Mignerey, S. Nabili, C. Palmer, C. Papageorgakis, M.M. Paranjpe, L. Wang

Massachusetts Institute of Technology, Cambridge, Massachusetts, USA

J. Bendavid, W. Busza, I.A. Cali, Y. Chen, M. D'Alfonso, J. Eysermans, C. Freer, G. Gomez-Ceballos, M. Goncharov, G. Grosso, P. Harris, D. Hoang, D. Kovalskyi, J. Krupa, L. Lavezzo, Y.-J. Lee, K. Long, C. Mironov, C. Paus, D. Rankin, C. Roland, G. Roland, S. Rothman, Z. Shi, G.S.F. Stephans, Z. Wang, B. Wyslouch, T. J. Yang

University of Minnesota, Minneapolis, Minnesota, USA

B. Crossman, B.M. Joshi, C. Kapsiak, M. Krohn, D. Mahon, J. Mans, B. Marzocchi, S. Pandey, M. Revering, R. Rusack, R. Saradhy, N. Schroeder, N. Strobbe, M.A. Wadud

University of Mississippi, Oxford, Mississippi, USA

L.M. Cremaldi

University of Nebraska-Lincoln, Lincoln, Nebraska, USA

K. Bloom, M. Bryson, D.R. Claes, G. Haza, J. Hossain, C. Joo, I. Kravchenko, J.E. Siado, W. Tabb, A. Vagnerini, A. Wightman, F. Yan, D. Yu

State University of New York at Buffalo, Buffalo, New York, USA

H. Bandyopadhyay, L. Hay, I. Iashvili, A. Kharchilava, M. Morris, D. Nguyen, S. Rappoccio, H. Rejeb Sfar, A. Williams

Northeastern University, Boston, Massachusetts, USA

G. Alverson, E. Barberis, J. Dervan, Y. Haddad, Y. Han, A. Krishna, J. Li, M. Lu, G. Madigan, R. Mccarthy, D.M. Morse, V. Nguyen, T. Orimoto, A. Parker, L. Skinnari, A. Tishelman-Charny, B. Wang, D. Wood

Northwestern University, Evanston, Illinois, USA

S. Bhattacharya, J. Bueghly, Z. Chen, K.A. Hahn, Y. Liu, Y. Miao, D.G. Monk, M.H. Schmitt, A. Taliercio, M. Velasco

University of Notre Dame, Notre Dame, Indiana, USA

G. Agarwal, R. Band, R. Bucci, S. Castells, A. Das, R. Goldouzian, M. Hildreth, K.W. Ho, K. Hurtado Anampa, T. Ivanov, C. Jessop, K. Lannon, J. Lawrence, N. Loukas, L. Lutton,

J. Mariano, N. Marinelli, I. Mcalister, T. McCauley, C. Mcgrady, C. Moore, Y. Musienko[16], H. Nelson, M. Osherson, A. Piccinelli, R. Ruchti, A. Townsend, Y. Wan, M. Wayne, H. Yockey, M. Zarucki, L. Zygala

The Ohio State University, Columbus, Ohio, USA

A. Basnet, B. Bylsma, M. Carrigan, L.S. Durkin, C. Hill, M. Joyce, M. Nunez Ornelas, K. Wei, B.L. Winer, B. R. Yates

Princeton University, Princeton, New Jersey, USA

F.M. Addesa, H. Bouchamaoui, P. Das, G. Dezoort, P. Elmer, A. Frankenthal, B. Greenberg, N. Haubrich, G. Kopp, S. Kwan, D. Lange, A. Loeliger, D. Marlow, I. Ojalvo, J. Olsen, A. Shevelev, D. Stickland, C. Tully

University of Puerto Rico, Mayaguez, Puerto Rico, USA

S. Malik

Purdue University, West Lafayette, Indiana, USA

A.S. Bakshi, V.E. Barnes, S. Chandra, R. Chawla, S. Das, A. Gu, L. Gutay, M. Jones, A.W. Jung, D. Kondratyev, A.M. Koshy, M. Liu, G. Negro, N. Neumeister, G. Paspalaki, S. Piperov, V. Scheurer, J.F. Schulte, M. Stojanovic, J. Thieman, A. K. Virdi, F. Wang, W. Xie

Purdue University Northwest, Hammond, Indiana, USA

J. Dolen, N. Parashar, A. Pathak

Rice University, Houston, Texas, USA

D. Acosta, T. Carnahan, K.M. Ecklund, P.J. Fernández Manteca, S. Freed, P. Gardner, F.J.M. Geurts, W. Li, O. Miguel Colin, B.P. Padley, R. Redjimi, J. Rotter, E. Yigitbasi, Y. Zhang

University of Rochester, Rochester, New York, USA

A. Bodek, P. de Barbaro, R. Demina, J.L. Dulemba, C. Fallon, A. Garcia-Bellido, O. Hindrichs, A. Khukhunaishvili, N. Parmar, P. Parygin[33], E. Popova[33], R. Taus, G.P. Van Onsem

The Rockefeller University, New York, New York, USA

K. Goulianos

Rutgers, The State University of New Jersey, Piscataway, New Jersey, USA

B. Chiarito, J.P. Chou, Y. Gershtein, E. Halkiadakis, A. Hart, M. Heindl, D. Jaroslawski, O. Karacheban[30], I. Laflotte, A. Lath, R. Montalvo, K. Nash, H. Routray, S. Salur, S. Schnetzer, S. Somalwar, R. Stone, S.A. Thayil, S. Thomas, J. Vora, H. Wang

University of Tennessee, Knoxville, Tennessee, USA

H. Acharya, D. Ally, A.G. Delannoy, S. Fiorendi, S. Higginbotham, T. Holmes, A.R. Kanuganti, N. Karunarathna, L. Lee, E. Nibigira, S. Spanier

Texas A&M University, College Station, Texas, USA

D. Aebi, M. Ahmad, O. Bouhali[96], M. Dalchenko, R. Eusebi, J. Gilmore, T. Huang, T. Kamon[97], H. Kim, S. Luo, S. Malhotra, R. Mueller, D. Overton, D. Rathjens, A. Safonov

Texas Tech University, Lubbock, Texas, USA

N. Akchurin, J. Damgov, V. Hegde, A. Hussain, Y. Kazhykarim, K. Lamichhane, S.W. Lee, A. Mankel, T. Peltola, I. Volobouev, A. Whitbeck

Vanderbilt University, Nashville, Tennessee, USA

E. Appelt, S. Greene, A. Gurrola, W. Johns, R. Kunnawalkam Elayavalli, A. Melo, F. Romeo, P. Sheldon, S. Tuo, J. Velkovska, J. Viinikainen

University of Virginia, Charlottesville, Virginia, USA

B. Cardwell, B. Cox, J. Hakala, R. Hirosky, A. Ledovskoy, C. Neu, C.E. Perez Lara

Wayne State University, Detroit, Michigan, USA

P.E. Karchin

University of Wisconsin - Madison, Madison, Wisconsin, USA

A. Aravind, S. Banerjee, K. Black, T. Bose, S. Dasu, I. De Bruyn, P. Everaerts, C. Galloni, H. He, M. Herndon, A. Herve, C.K. Koraka, A. Lanaro, R. Loveless, J. Madhusudanan Sreekala, A. Mallampalli, A. Mohammadi, S. Mondal, G. Parida, D. Pinna, A. Savin, V. Shang, V. Sharma, W.H. Smith, D. Teague, H.F. Tsoi, W. Vetens, A. Warden

Authors affiliated with an institute or an international laboratory covered by a cooperation agreement with CERN

S. Afanasiev, V. Andreev, Yu. Andreev, T. Aushev, M. Azarkin, A. Babaev, A. Belyaev, V. Blinov[98], E. Boos, V. Borshch, D. Budkouski, V. Chekhovsky, R. Chistov[98], A. Dermenev, T. Dimova[98], D. Druzhkin[99], M. Dubinin[89], L. Dudko, A. Ershov, G. Gavrilov, V. Gavrilov, S. Gninenko, V. Golovtcov, N. Golubev, I. Golutvin, I. Gorbunov, A. Gribushin, Y. Ivanov, V. Kachanov, A. Kaminskiy, V. Karjavine, A. Karneyeu, V. Kim[98], M. Kirakosyan, D. Kirpichnikov, M. Kirsanov, V. Klyukhin, O. Kodolova[100], V. Korenkov, A. Kozyrev[98], N. Krasnikov, A. Lanev, P. Levchenko[101], N. Lychkovskaya, V. Makarenko, A. Malakhov, V. Matveev[98], V. Murzin, A. Nikitenko[102,100], S. Obraztsov, V. Oreshkin, V. Palichik, V. Perelygin, S. Petrushanko, S. Polikarpov[98], V. Popov, O. Radchenko[98], V. Rusinov, M. Savina, V. Savrin, V. Shalaev, S. Shmatov, S. Shulha, Y. Skovpen[98], S. Slabospitskii, V. Smirnov, A. Snigirev, D. Sosnov, V. Sulimov, E. Tcherniaev, A. Terkulov, O. Teryaev, I. Tlisova, A. Toropin, L. Uvarov, A. Uzunian, A. Vorobyev[†], N. Voytishin, B.S. Yuldashev[103], A. Zarubin, I. Zhizhin, A. Zhokin

[†] *Deceased*
[1] *Also at Yerevan State University, Yerevan, Armenia*
[2] *Also at TU Wien, Vienna, Austria*
[3] *Also at Institute of Basic and Applied Sciences, Faculty of Engineering, Arab Academy for Science, Technology and Maritime Transport, Alexandria, Egypt*
[4] *Also at Ghent University, Ghent, Belgium*
[5] *Also at Universidade Estadual de Campinas, Campinas, Brazil*
[6] *Also at Federal University of Rio Grande do Sul, Porto Alegre, Brazil*
[7] *Also at UFMS, Nova Andradina, Brazil*
[8] *Also at Nanjing Normal University, Nanjing, China*
[9] *Now at The University of Iowa, Iowa City, Iowa, USA*

2024 JINST 19 P09012

[10] *Also at University of Chinese Academy of Sciences, Beijing, China*
[11] *Also at China Center of Advanced Science and Technology, Beijing, China*
[12] *Also at University of Chinese Academy of Sciences, Beijing, China*
[13] *Also at China Spallation Neutron Source, Guangdong, China*
[14] *Now at Henan Normal University, Xinxiang, China*
[15] *Also at Université Libre de Bruxelles, Bruxelles, Belgium*
[16] *Also at an institute or an international laboratory covered by a cooperation agreement with CERN*
[17] *Now at British University in Egypt, Cairo, Egypt*
[18] *Now at Cairo University, Cairo, Egypt*
[19] *Also at Birla Institute of Technology, Mesra, Mesra, India*
[20] *Also at Purdue University, West Lafayette, Indiana, USA*
[21] *Also at Université de Haute Alsace, Mulhouse, France*
[22] *Also at Department of Physics, Tsinghua University, Beijing, China*
[23] *Also at Ilia State University, Tbilisi, Georgia*
[24] *Also at The University of the State of Amazonas, Manaus, Brazil*
[25] *Also at Erzincan Binali Yildirim University, Erzincan, Turkey*
[26] *Also at University of Hamburg, Hamburg, Germany*
[27] *Also at RWTH Aachen University, III. Physikalisches Institut A, Aachen, Germany*
[28] *Also at Isfahan University of Technology, Isfahan, Iran*
[29] *Also at Bergische University Wuppertal (BUW), Wuppertal, Germany*
[30] *Also at Brandenburg University of Technology, Cottbus, Germany*
[31] *Also at Forschungszentrum Jülich, Juelich, Germany*
[32] *Also at CERN, European Organization for Nuclear Research, Geneva, Switzerland*
[33] *Now at an institute or an international laboratory covered by a cooperation agreement with CERN*
[34] *Also at Institute of Physics, University of Debrecen, Debrecen, Hungary*
[35] *Also at Institute of Nuclear Research ATOMKI, Debrecen, Hungary*
[36] *Now at Universitatea Babes-Bolyai - Facultatea de Fizica, Cluj-Napoca, Romania*
[37] *Also at Physics Department, Faculty of Science, Assiut University, Assiut, Egypt*
[38] *Also at HUN-REN Wigner Research Centre for Physics, Budapest, Hungary*
[39] *Also at Punjab Agricultural University, Ludhiana, India*
[40] *Also at University of Visva-Bharati, Santiniketan, India*
[41] *Also at Indian Institute of Science (IISc), Bangalore, India*
[42] *Also at IIT Bhubaneswar, Bhubaneswar, India*
[43] *Also at Institute of Physics, Bhubaneswar, India*
[44] *Also at University of Hyderabad, Hyderabad, India*
[45] *Also at Deutsches Elektronen-Synchrotron, Hamburg, Germany*
[46] *Also at Department of Physics, Isfahan University of Technology, Isfahan, Iran*
[47] *Also at Sharif University of Technology, Tehran, Iran*
[48] *Also at Department of Physics, University of Science and Technology of Mazandaran, Behshahr, Iran*
[49] *Also at Helwan University, Cairo, Egypt*
[50] *Also at Italian National Agency for New Technologies, Energy and Sustainable Economic Development, Bologna, Italy*
[51] *Also at Centro Siciliano di Fisica Nucleare e di Struttura Della Materia, Catania, Italy*
[52] *Also at Università degli Studi Guglielmo Marconi, Roma, Italy*
[53] *Also at Scuola Superiore Meridionale, Università di Napoli 'Federico II', Napoli, Italy*
[54] *Also at Fermi National Accelerator Laboratory, Batavia, Illinois, USA*
[55] *Also at Laboratori Nazionali di Legnaro dell'INFN, Legnaro, Italy*
[56] *Also at Ain Shams University, Cairo, Egypt*
[57] *Also at Consiglio Nazionale delle Ricerche - Istituto Officina dei Materiali, Perugia, Italy*
[58] *Also at Riga Technical University, Riga, Latvia*
[59] *Also at Department of Applied Physics, Faculty of Science and Technology, Universiti Kebangsaan Malaysia, Bangi, Malaysia*
[60] *Also at Consejo Nacional de Ciencia y Tecnología, Mexico City, Mexico*
[61] *Also at Trincomalee Campus, Eastern University, Sri Lanka, Nilaveli, Sri Lanka*

2024 JINST 19 P09012

[62] *Also at Saegis Campus, Nugegoda, Sri Lanka*
[63] *Also at INFN Sezione di Pavia, Università di Pavia, Pavia, Italy*
[64] *Also at National and Kapodistrian University of Athens, Athens, Greece*
[65] *Also at Ecole Polytechnique Fédérale Lausanne, Lausanne, Switzerland*
[66] *Also at Universität Zürich, Zurich, Switzerland*
[67] *Also at Stefan Meyer Institute for Subatomic Physics, Vienna, Austria*
[68] *Also at Laboratoire d'Annecy-le-Vieux de Physique des Particules, IN2P3-CNRS, Annecy-le-Vieux, France*
[69] *Also at Near East University, Research Center of Experimental Health Science, Mersin, Turkey*
[70] *Also at Konya Technical University, Konya, Turkey*
[71] *Also at Izmir Bakircay University, Izmir, Turkey*
[72] *Also at Adiyaman University, Adiyaman, Turkey*
[73] *Also at Bozok Universitetesi Rektörlügü, Yozgat, Turkey*
[74] *Also at Marmara University, Istanbul, Turkey*
[75] *Also at Milli Savunma University, Istanbul, Turkey*
[76] *Also at Kafkas University, Kars, Turkey*
[77] *Now at Istanbul Okan University, Istanbul, Turkey*
[78] *Also at Hacettepe University, Ankara, Turkey*
[79] *Also at Istanbul University - Cerrahpasa, Faculty of Engineering, Istanbul, Turkey*
[80] *Also at Yildiz Technical University, Istanbul, Turkey*
[81] *Also at Vrije Universiteit Brussel, Brussel, Belgium*
[82] *Also at School of Physics and Astronomy, University of Southampton, Southampton, United Kingdom*
[83] *Also at University of Bristol, Bristol, United Kingdom*
[84] *Also at IPPP Durham University, Durham, United Kingdom*
[85] *Also at Monash University, Faculty of Science, Clayton, Australia*
[86] *Also at Università di Torino, Torino, Italy*
[87] *Also at Bethel University, St. Paul, Minnesota, USA*
[88] *Also at Karamanoğlu Mehmetbey University, Karaman, Turkey*
[89] *Also at California Institute of Technology, Pasadena, California, USA*
[90] *Also at United States Naval Academy, Annapolis, Maryland, USA*
[91] *Also at Bingol University, Bingol, Turkey*
[92] *Also at Georgian Technical University, Tbilisi, Georgia*
[93] *Also at Sinop University, Sinop, Turkey*
[94] *Also at Erciyes University, Kayseri, Turkey*
[95] *Also at Horia Hulubei National Institute of Physics and Nuclear Engineering (IFIN-HH), Bucharest, Romania*
[96] *Also at Texas A&M University at Qatar, Doha, Qatar*
[97] *Also at Kyungpook National University, Daegu, Korea*
[98] *Also at another institute or international laboratory covered by a cooperation agreement with CERN*
[99] *Also at Universiteit Antwerpen, Antwerpen, Belgium*
[100] *Also at Yerevan Physics Institute, Yerevan, Armenia*
[101] *Also at Northeastern University, Boston, Massachusetts, USA*
[102] *Also at Imperial College, London, United Kingdom*
[103] *Also at Institute of Nuclear Physics of the Uzbekistan Academy of Sciences, Tashkent, Uzbekistan*

2024 JINST 19 P09012